Accepted Manuscript

Mechanical stratigraphy influence on fault-related folds development: Insights from the Cantabrian Zone (NW Iberian Peninsula)

Mayte Bulnes, Josep Poblet, Hodei Uzkeda, Indira Rodríguez-álvarez

PII: S0191-8141(18)30229-3

DOI: 10.1016/j.jsg.2018.10.002

Reference: SG 3753

To appear in: *Journal of Structural Geology*

Received Date: 23 April 2018

Revised Date: 2 October 2018

Accepted Date: 2 October 2018

Please cite this article as: Bulnes, M., Poblet, J., Uzkeda, H., Rodríguez-álvarez, I., Mechanical stratigraphy influence on fault-related folds development: Insights from the Cantabrian Zone (NW Iberian Peninsula), *Journal of Structural Geology* (2018), doi: https://doi.org/10.1016/j.jsg.2018.10.002.

Mechanical stratigraphy influence on fault-related folds development: insights from the Cantabrian Zone (NW Iberian Peninsula)

Mayte BULNES [1], Josep POBLET [1], Hodei UZKEDA [1,*] and Indira RODRÍGUEZ-ÁLVAREZ [1]

[1] Departamento de Geología, Universidad de Oviedo, C/Jesús Arias de Velasco s/n, 33005 Oviedo, Spain, EU

E-mail: maite@geol.uniovi.es, jpoblet@geol.uniovi.es, hodei@geol.uniovi.es[*] (corresponding author, phone +34 985103120), indira@geol.uniovi.es

KEYWORDS

Cantabrian Zone, Carboniferous griotte limestones, detachment folds, fault-bend folds, fault-propagation folds, mechanical stratigraphy

ABSTRACT

An excellently exposed outcrop of Carboniferous rocks in the Cantabrian Zone (Variscan foreland fold-thrust belt in NW Iberia) displays fault-bend, fault-propagation and detachment folds. To unravel the parameters that controlled their development, we constructed detailed cross-sections and analysed them. Detachment folds exhibit the greatest amounts of layer-parallel/bulk strain, forelimb dip and forelimb/hinge thickening and the lowest interlimb angle, whereas fault-bend folds have the lowest values except for the interlimb angle, with fault-propagation folds exhibiting intermediate values. The forelimbs of all these folds show some strain and thickening, and the detachment folds also show thickening and strain in the hinge area. Mechanical stratigraphy was determined to be the main controlling factor on the fold/thrust style; ramp folds developed in thick-bedded, isotropic, relatively strong and brittle rocks, whereas detachment folds developed in a thin-bedded, anisotropic, relatively weak and ductile unit. Competent rocks and smooth bedding surfaces induced fault-bend folding, whereas less competent and rough bedding surfaces favoured fault-propagation folding. The main detachments are located at the boundaries between mechanical units with substantial changes in their mechanical properties. The size of the structures depends on the occurrence of a basal detachment, variety of lithologies with different competences and smoothness of bedding surfaces.

1. INTRODUCTION

Although many types of fold/thrust interaction have been described in the literature, thrust-related folds are usually classified into three basic types: fault-bend folds, fault-propagation folds and detachment folds (e.g., Suppe, 1985; Jamison, 1987; Poblet, 2004; Shaw et al., 2005; Nemcok et al., 2009; McClay, 2011; Brandes and Tanner, 2014). Fault-bend folds (Rich, 1934) form as a result of the movement of a fault block along a non-planar fault surface, which causes the bending of the fault block, and therefore, the formation of the fold. Although they usually develop in the hangingwall, they can also develop in the footwall or in both fault blocks. Fault-propagation folds (Dahlstrom, 1970) are formed contemporaneously with the propagation of a fault in a ramp situation through a series of strata, so that the shortening causes the formation of a fold near its termination. Detachment or décollement folds (Chamberlin, 1910), unlike fault-bend and fault-propagation folds, are not associated with a fault ramp, but form in relation to a thrust parallel to the layers (detachment). They can be generated near the thrust tip or in any other area along the thrust if a sharp decrease in the amount of displacement occurs. Detachment folds may be limited by a lower detachment, by an upper one or by both. These three styles of fold/thrust interaction exhibit several distinguishing features in terms of:

a) Fold geometry. Assuming that thrust faults involve undeformed rocks and subsequent deformation is absent, fault-bend folds are usually open structures with gently dipping limbs, fault-propagation folds are usually tighter structures with a long, gently dipping backlimb and a shorter, steeply dipping forelimb, and detachment folds exhibit all sorts of geometries.

b) Fault geometry. Fault-bend and fault-propagation folds are ramp folds, whereas detachment folds are unrelated to thrust ramps.

c) Fault tip. Fault-bend folds and some detachment folds are not related to a thrust tip, whereas fault-propagation and some detachment folds are related to a thrust tip.

d) Fault displacement. The fault displacement is almost constant in fault-bend folds, although it slightly decreases towards the forelimb because part of the deformation is consumed in bending of the rocks, whereas a fault displacement gradient decreasing up to zero at the fault tip occurs in fault-propagation folds and in some detachment folds.

e) Fold/fault timing. Thrust fault formation is previous to folding in fault-bend folds, but both are simultaneous in fault-propagation folds and in detachment folds.

These three types of structures are common in nature and, although some fold and thrust belts exhibit one predominant style, they are usually developed in all fold and thrust belts and other tectonic settings around the world irrespective of their age (e.g., McClay, 1992, 2004; Mitra and Fisher, 1992; Anastasio et al., 1997; Lisle and Poblet, 2010; Poblet and Lisle, 2011). Despite the significant differences between these three types of structures, they are often found in close spatial and temporal association with each other, and therefore, the occurrence of one or another structure demands an explanation.

The main factors that control the development of fault-bend folds, fault-propagation folds and detachment folds or the predominance of thrust faulting versus folding have been investigated using different sorts of techniques: fieldwork in natural examples (Chester, 2003); laboratory rock models (Chester et al., 1991); laboratory sand, plasticine and silicon putty models (Dixon and Liu, 1992; Liu and Dixon, 1995; Storti et al., 1997; Yan et al., 2016; Li and Mitra, 2017); stress models (Jamison, 1992); geometrical models (Stewart, 1996); finite element models (Albertz and Lingrey, 2012); and discrete-element models (Hughes et al., 2014) amongst others.

Chester et al. (1991) concluded that the preferential development of a specific fold/thrust style depends on the fault zone drag, bending and shearing resistance of the hanging wall, shear strength of layer interfaces and loading conditions (expressed as the strength ratio of the resistance to foreland translation relative to the resistance to internal shortening of the sheet), and on the anisotropy of the layers. Thus, low strength ratios favour fault-bend folding, whereas high strength ratios favour internal shortening of the sheet; isotropic and thick units above a propagating thrust tip will shorten primarily by faulting, whereas thinly layered, anisotropic units will shorten by fault-propagation folding. According to Dixon and Liu (1992), Liu and Dixon (1995), Storti et al. (1997) and Yan et al. (2016) the fold/thrust style is a function of the stage of evolution of the structures: a) they initiate as décollement folds and progressively become fault-propagation folds, and b) subsequently they become fault-bend folds by décollements breaking and ramping up and flattening into upper décollements. According to Jamison (1992) the development of a specific fold/thrust style is a competition between buckling and faulting, which are represented by instability surfaces controlled by the mechanical stratigraphy. The fold/thrust style depends upon which instability surface is intersected first by the stress path controlled by the burial depth and regional tectonics. Detachment folds develop mainly in the shallow subsurface whereas fault-bend folds dominate the deeper subsurface. Stewart (1996) concluded that amplification of a detachment fold requires filling its core with ductile material, so if it is insufficient, fold growth would be inhibited and eventual thrusting would accommodate shortening. According to Chester (2003) the mechanical interaction between the structural lithic units and boundary conditions imposed on them define the fold/thrust style. Where two units, both formed by a relatively weak, ductile, anisotropic lower section and a relatively strong, brittle, more isotropic upper section, were stacked within the thrust sheet, inverted fault–propagation folds formed in the centre of each unit, and the overall transition upward from close- to wide-spaced folds and imbricate faults developed in the multilayer. Where the upper unit was isolated, deformation was dominated by imbricate faulting with little associated folding, and inverted fault–propagation folds did not form. According to Albertz and Lingrey (2012) mechanical stratigraphy, initial fault dip and inter-layer detachments affect fault propagation and control fold geometry. Uniform sandstones exhibit efficient strain localization and patterns of fault tip propagation, whereas uniform shales tend to inhibit fault propagation due to distributed plastic deformation, and mixed inter-layered sandstone and shale deform in a disharmonic manner. Detachments accommodate shortening by bed-parallel slip, resulting in fault-bend fold kinematics and poorly expressed fault propagation across layers. Hughes et al. (2014) concluded that frictional properties of the upper detachment and the mobility of the foreland wall exert the strongest influence on structural style. Fault dip, mechanical layer spacing, and relative mechanical layer strength all have a secondary influence. Overall material strength, the presence or absence of particle rebonding and sedimentation rate have negligible effects on structural style. They found that fault-bend folding is favoured at low fault ramp dips, with thinly spaced mechanical layers, and strong layer strength contrasts. In contrast, increased friction and a fixed foreland boundary inhibit slip on a potential upper detachment surface and encourage fault-propagation folding. Moreover, steeper fault dips, more widely spaced mechanical layers, and decreased layer strength contrast leads to structures that deform by a mixture of fault-bend and fault-propagation folding. According to Li and Mitra (2017) fold-thrust belts formed above a ductile detachment typically contain detachment folds, whereas those formed above frictional detachments contain fault-related fold complexes, such as ramp folds.

While previous studies have lent significant insight into the processes governing fault-related folding style in different contractional settings, further detailed field observations of natural examples of the relationship between rock properties and structural style are of substantial value as a means of testing the applicability of previous findings. The Cantabrian Zone (foreland fold and thrust belt of the Variscan orogeny in the NW Iberian Peninsula) (Fig. 1a) has particular value for comparative purposes because it hosts the full range of structural styles of interest, that vary both at local and regional-scale, and involves many different types of rocks. At large scale, in the western portion of the Cantabrian Zone, there is a transition from a southern region mainly dominated by thrusts to a northern zone where folds predominate (e.g., Soler, 1967; Julivert and Arboleya, 1984; Alonso et al., 1991; Bulnes and Aller, 2002). Fault-bend folds are the main structures in the southern region, whereas thrust-tip folds dominate in the northern one. In addition, in both regions the three types of thrust-related folds coexist at smaller scale. In the southern branch of this belt, there is an excellently exposed outcrop of Carboniferous rocks, where different fold/thrust styles occur; this outcrop will be the object of study in this work. Detailed quantitative analyses of outcrops, as presented in this study, provide a rigorous basis for comparison with recent model-based studies.

The methodology followed in this work includes: construction of a detailed stratigraphic section; measurement in the field of the orientation of beds, faults and fold elements, as well as fault slip and bed thickness; construction of geological cross-sections with the aid of photo-geological interpretations corrected to become proper geological profiles; geometrical and fault displacement analysis; and estimations of shortening, layer-parallel strain and bulk strain using the collected data.

2. GEOLOGICAL SETTING

Cantabrian Zone is the name given to the foreland fold and thrust belt of the Variscan orogen in NW Iberian Peninsula developed during Carboniferous times (Fig. 1a). This belt consists of an orogenic wedge that involves from Cambrian to

Carboniferous rocks, thins towards the foreland (eastwards) in cross-sectional view and is made up of different kilometre-scale thrust sheets. This belt developed under diagenetic conditions, so that only some areas were affected by metamorphism of low or very low grade, and cleavage is only present in some particular locations. Different types of thrusts systems, such as imbricate fans and duplex, and different types of thrust-related folds, such as fault-bend, fault-propagation and detachment folds, are the most common structures documented in different portions of the belt (e.g., Julivert, 1971a, 1979, 1981, 1983; Savage, 1979, 1981; Pérez-Estaún et al., 1988; Pérez-Estaún and Bastida, 1990; Aller et al., 2004; Alonso et al., 2009 and references therein). A number of thrusts and related folds are not in their original position but sub-vertical or overturned due to piling up of different structural units and subsequent folding. The Cantabrian Zone has an arcuate geometry around an approximately E-W axis in map view because it is located in the core of an orocline called Ibero-Armorican or Asturian Arc first recognized by Suess (1892) (Fig. 1a). The Cantabrian Mountains were uplifted during Cenozoic times due to the Alpine contraction that affected the north margin of the Iberian Peninsula (Alonso et al., 1996). This resulted in reactivation of previous Paleozoic and Mesozoic structures, and, to less extent, development of new ones (Pulgar et al., 1999).

The studied outcrop is located in the southwest portion of the Cantabrian Zone and belongs to the Sobia-Bodón structural unit according to Julivert (1971a) or to the Bodón-Ponga structural unit according to Alonso et al. (2009), in the southern branch of the Ibero-Armorican Arc (Figs. 1a and 1b). In particular, the outcrop is located in the north limb of the Villasecino anticline, a kilometre-scale, tight and approximately upright anticline that strikes E–W (Figs. 1c and 1d). This regional-scale anticline is interpreted to be a Variscan fold that involves a Cambrian to Carboniferous stratigraphic succession as can be observed in several geological maps and cross sections (e.g., De Sitter, 1962; Marcos, 1968; Martínez-Álvarez et al., 1968; Alonso et al., 1989; Rodríguez-Fernández et al., 1990; Instituto Geológico y Minero de España, 2005-2011). The studied outcrop is located along the east side of a NNE-SSW local road close to the small locality of San Emiliano and to the east of Villasecino, province of León, Spain (Fig. 1c). It is an approximately 35 m long and 12 m high slope inclined about 80° to the WNW (Fig. 2a).

3. MECHANICAL STRATIGRAPHY

The rocks studied in the outcrop belong to the Alba (or Genicera) Fm., colloquially known as “Carboniferous griotte limestone”. Initially this formation was called "Griotte limestone" by Prado and Verneuil (1850), "Griotte marble" by Barrois (1882), and "Griotte of Puente de Alba" by Comte (1959). Ginkel (1965) renamed it as Alba Fm. Winkler Prins (1968) subdivided it into three members, which were named Gorgera, Lavandera and Canalon by Wagner et al. (1971) who also changed the name of this formation to Genicera Fm.

The Alba Fm. is underlain by the Vegamián Fm., a very thin level of dark grey slates with occasional manganese nodules, cherts and sandstones, which, in turn, is underlain by the Baleas Fm. formed by coarse-grained, bioclastic limestones whose colour ranges from light grey to white with red fringes. The Alba Fm. is overlain by the Barcaliente Fm. made up of fine-grained, dark grey limestones.

The three members of the Alba Fm. are described below from bottom to top (Figs. 2a and 2b). In the study area, the Gorgera Mb. is formed by red, nodular, wackestone limestones (griotte facies) with scarce red slate interbeds. The Lavandera Mb. is composed of red to grey radiolarites and red, grey-greenish, beige siliceous slates. The Canalón Mb. is formed by red, nodular, wackestone limestones (griotte facies) and grey, mudstone limestones with interbedded red and grey-greenish slates at the lower part becoming light grey, mudstone limestones with occasional grey-greenish slate interbeds up section. Marine bioclasts such as planktonic organisms, ostracods, gasteropods, trilobites and goniatites (Rodríguez-Fernández et al., 1991) are frequent.

From the mechanical point of view the studied outcrop has been divided into four distinctive structural lithic units in the sense of Currie et al. (1962), i.e., packages of beds that display a characteristic reaction to deformation. These units are listed below from bottom to top (Figs. 2a and 2b). 1) Red, nodular, limestones (griotte) with occasional slate interbeds. 2) Alternations of radiolarites and slates. 3) Alternations of red, nodular, limestones (griotte) and grey limestones with interbedded slates. 4) Grey limestones with scarce slate interbeds. From the rock features point of view, the main elements employed to define these units are the lithology types, the average grain size of the rocks, the erosion resistance, the bed thickness and the morphology of the bedding surfaces. For instance, the radiolarites and slates unit and the grey limestones unit are formed by fine-grained rocks, however, the griotte limestones unit is made up of medium-grained rocks. The radiolarites and slates unit includes between 35 and 65% of competent rocks (radiolarites), whereas both the griotte limestones unit and the grey limestones unit have almost no incompetent rocks (slates). Average bedding thickness is 15-20 cm for the griotte limestones unit, around 15 cm for the grey limestones unit and around 5 cm for the radiolarites and slates unit. Bedding surfaces within the griotte limestones unit are relatively rough, whereas they are smooth in the radiolarites and slates unit and in the grey limestones unit.

To visualize the differences between the mechanical units defined, a normalized value between 1 and 4 has been assigned to each of the following representative parameters: average grain size, percentage of competent rocks, erosion resistance, bed thickness and bed roughness, assuming that limestones and radiolarites are competent rocks whereas slates are incompetent rocks. Values close to 1 for a specific parameter indicate that the mechanical unit has a low value for this parameter, whereas values close to 4 indicate high numbers. They have been assigned according to the logs depicted in the stratigraphic column in figure 2b. These values have been plotted for each mechanical unit in a pentagonal diagram in which each of the radii of the pentagon represents one of the estimated parameters (Fig. 2c). In the pentagonal diagram, the unit formed by radiolarites and slates, which is supposed to be the most incompetent unit, is represented as a pentagon of small dimensions, the griotte limestones unit, an intermediate competence unit, as a larger pentagon, and the grey limestones unit, probably the most competent unit, as a triangle. The unit composed of griotte limestones, grey limestones and slates is depicted as a pentagon of intermediate size in between the griotte limestones unit and the radiolarites and slates unit since it includes a mixture of lithologies from other units.

4. STRUCTURE

The general dip of the beds in the studied outcrop is approximately constant from 70° to 80° to the NNE (Figs. 3a and 3b). Different types of structures, such as faults, folds, cleavage, veins and joints affect the four mechanical units described above. The main structures developed within mechanical units 1 and 4 are faults subparallel to bedding, except in some sectors where they are slightly oblique to it, and some folds. Mechanical unit 2 is bounded by detachments both towards the south-southwest and towards the north-northeast. Folds and numerous fold-accommodation faults predominate within this unit. There are almost no structures within mechanical unit 3.

Some long faults subperpendicular to the stratification cut and offset mechanical units 2, 3 and 4.

4.1. Original disposition of the structures

The orientation of the structures and the manner they are arranged in the studied outcrop makes it difficult to interpret it from the structural point of view. Thus, folds and faults exhibit different dips and strikes, normal faults coexist with reverse faults and cross-cutting relationships between them are unclear (Fig. 3b). Considering that this outcrop is located in the north limb of the larger-scale Villasecino anticline (Figs. 1c, 1d and 4a), Masini et al. (2010a) suggested that the structures developed in the Gorgera Mb. could have been developed either before the initiation of the Villasecino anticline or during an early stage of amplification of the anticline as fold-accommodation structures. Assuming that this hypothesis is valid for the whole outcrop, in order to properly visualize the relationships between structures and bedding, as well as the relationships between different types of structures and their nature (contractional, extensional, strike slip), the geological interpretation of the outcrop was rotated 80° in a clockwise sense looking ESE around a horizontal ESE–WNW axis (Fig. 4b). The operation performed consists of rotating this portion of the north limb of the Villasecino anticline around its own fold axis as a rigid body. In the rotated geological interpretation of the studied outcrop: a) many faults become thrust faults, some of them north-directed and some of them south-directed; b) the faults bounding different mechanical units become subhorizontal detachments; and c) the geometrical relationships between folds and faults can be easily interpreted in terms of thrust-related folding in agreement with the structural style mapped in surrounding areas and in the rest of the Cantabrian fold and thrust belt. However, the orientation of a few faults does not make sense in the rotated geological interpretation as we will discuss below.

The NNE-SSW strike of the outcrop (Fig. 3) is approximately perpendicular to that of both folded bedding (Figs. 5a, 5b and 5c) and thrust surfaces (Fig. 5d). However, the outcrop face dips steeply towards the WNW (Fig. 3), whereas the fold axes are sub-horizontal to gently plunging towards the WNW (Figs. 5a, 5b and 5c). Thus, the geological cross-sections constructed in the field with the help of outcrop photographs, were corrected using a Ramsay and Huber (1987) method and with the aid of the software Move (Midland Valley) to obtain profiles perpendicular to the fold axes which allow a proper visualization of the thrust-related folds identified in the studied outcrop. Since the outcrop face and the fold axes exhibit slightly different orientations in different portions of the outcrop (Figs. 5a, 5b and 5c), a geological profile for each mechanical unit was constructed using average fold axes estimated (Fig. 6). The contractional structures will be described below using the rotated and corrected geological profiles in figure 6, and the description will be carried out from south to north, that is, from the lowest to the uppermost mechanical unit.

4.2. Fault-propagation fold

The lowermost studied structure is a detachment that separates the griotte limestones unit from the underlying Baleas Fm. limestones through the black slates of the Vegamián Fm. Both the griotte limestones and the Vegamián Fm. slates are approximately parallel to each other. Whereas in the field the griotte limestones do not exhibit a particular intense deformation in the vicinity of the contact with the black slates, the slates are strongly deformed as evidenced by the occurrence of centimetre-scale shear bands, veins and folds.

The most important structure involving the griotte limestones unit is a parallel, open anticline, with rounded geometry (Fig. 6a). Its fold width is greater than 8 m and its amplitude is greater than 2 m. This fold is asymmetric and south-vergent, so that the southern limb (forelimb) dips steeply (around 60°) and is shorter than the northern limb (backlimb) which is longer and dips moderately (around 30°). The occurrence of calcite slickensides along decimetre-spaced bedding surfaces in the fold backlimb suggest that flexural slip was one of the mechanisms responsible for the distribution of deformation within folded layers. This anticline is developed in the hangingwall of a south-directed thrust fault that dips moderately to the north and whose maximum fault displacement measured in the geological profile is almost 4 m. The lower beds of the griotte limestones unit overthrust themselves in a hangwingwall flat over a footwall ramp situation. Towards the south and up section, the thrust bifurcates into a set of smaller displacement thrusts that offset the upper beds of the griotte limestone unit in a hangingwall ramp over a footwall ramp situation. Where the main thrust bifurcates, some smaller-scale, open anticlines and synclines occur. These minor folds are interpreted as ductile structures accommodating thrust displacements up section. The main fold geometry, the fold-thrust relationships and the thrust displacement pattern suggest that the whole structure can be interpreted as a ramp fold, in particular a fault-propagation fold developed over a slightly deformed footwall, with intense forelimb deformation accommodated by second-order folding and thrusting. We interpret that the main thrust responsible for the fault-propagation fold emanates from the detachment located at the base of the griotte limestones (Masini et al., 2010a, 2010b).

To verify quantitatively whether this structure could be modelled as a fault-propagation fold (Suppe and Medwedeff, 1990): a) the interlimb angle and the thrust ramp dip were measured and plotted on a Jamison (1987) chart for fault-propagation folds (Fig. 7a), and b) the displacement on the fault for different horizons and the distance from each cut-off point to an arbitrary reference point measured on the fault were obtained and plotted on the Chapman and Williams (1984) graph (Fig. 8a). According to the Jamison (1987) graph, the studied fold can be interpreted as a fault-propagation fold with a slight forelimb thickening, which actually occurs in the field example. According to the Chapman and Williams (1984) graph, the thrust displacement decreases up section following the typical pattern for fault-propagation folds (e.g., McConnell et al., 1997). The curved geometry of the function on the distance/displacement diagram (Fig. 8a) may be due to one the following factors: a) the thrust propagation to slip ratio (P/S) is not constant (according to Hughes and Shaw, 2014 the gradient in displacement is linear in models of fault-propagation folds with constant P/S ratio), b) the smoothly curved morphology of the thrust surface (Fig. 6a), c) as we will see below, the fault-propagation fold analysed does not correspond exactly to a trishear fault-propagation fold or to a fault-propagation fold with a fixed-axial surface (according to Hughes and Shaw, 2014 the gradient in displacement is linear in those models of fault-propagation folds), or d) combinations of the factors described above.

Two main characteristics of this fault-propagation fold suggest that it might be interpreted as a trishear fault-propagation fold: a) the forelimb region resembles a triangular zone of maximum deformation in terms of amount of thrust faults and folds, as well as strain (see paragraphs below), whose apex emanates from the main fault and widens up section away from it towards the south; and b) the forelimb thickness is greater than that of the backlimb reaching around 110 %. In order to unravel the evolution of this structure and quantify its controlling parameters, forward models of trishear fault-propagation folds were constructed using the modules implemented in the software Geosec based on the Erslev (1991) and Allmendinger (1998) models. The goal was to obtain a model that emulates the geometry of the actual fault-propagation fold by iterating the values of the different parameters. The input parameters employed have been measured in the field and in the geological profile depicted in figure 6a, and derived from the lost area diagram (Fig. 9a). Unfortunately, it was not possible to obtain a model of a trishear fault-propagation fold that successfully reproduces the geometry of the actual fault-propagation fold developed in the griotte limestones in terms of crestal width, triangular zone position and forelimb dip.

Since this structure could not be successfully modelled as a tri-shear fault-propagation fold, we tried to model it following another type of kinematic approach. Taking into account that the layer thickness is not constant (the ratio between the backlimb thickness divided by the forelimb thickness is approximately 0.94), an attempt was made to model this structure as a fixed-axial surface fault-propagation fold with differential-bedding angular shear (Suppe and Medwedeff, 1990, Mossar and Suppe, 1992). The input parameters have been measured in the field and in the geological profile depicted in figure 6a. These values have been plotted on the graph in figure 9 of Mossar and Suppe (1992). The results suggest that this structure resembles a fault-propagation fold with a fixed-axial surface and a moderate amount of positive angular shear, i.e. the loose line in the layers offset by the thrust is inclined in the same direction as the thrust. This result is in accordance with the restoration of this structure shown in figure 7 of Masini et al. (2010) in which the loose line in the layers offset by the thrusts is not vertical but inclined because the lower layers have a greater length than the upper ones. However, the forelimb dip is strictly parallel to the backlimb axial surface in the theoretical models of fault-propagation folds generated according to the fixed-axial surface theory, whereas in the studied example they form an angle of approximately 10°.

To quantify the amount of layer-parallel strain experienced by the horizons involved in the fault-propagation fold we followed a strategy proposed by Groshong (2015). First we measured the unfolded bed length of various horizons involved in the fault-propagation fold (L1) as well as the width of the structure (W), in the geological profile presented in figure 6a (Table 1). Secondly we estimated the shortening undergone by the structure (S) using the lost area diagram of Epard and Groshong (1993), i.e., the slope of the best-fit function for the excess area versus height of different horizons with respect to an arbitrary reference level (Fig. 9a). Both the excess area and the height were estimated using the geological profile in figure 6a. The x value of the intersection between the best-fit function and the x axis supplies the estimated depth to detachment. Since the difference between the depth to detachment estimated from the lost area diagram and the actual depth in the field is almost 1 cm (Fig. 9a), it is reasonable to think that the lost area diagram supplied correct results, and therefore, the shortening estimate is correct. Furthermore, the fact that the estimated depth to detachment and the actual one are virtually identical validates the geological profile from the cross-sectional area point of view. The next step was estimating the initial bed length before deformation (Lo) as (Groshong and Epard, 1994):

$$Lo = W + S \quad (1).$$

Finally we estimated the layer-parallel strain each horizon suffered (Lps) using the following equation (Groshong and Epard, 1994):

$$Lps = (L1 - Lo) / Lo \quad (2).$$

The percentages of layer-parallel strain estimated for the lower horizons of the stratigraphic succession are less than 1%, and therefore, they can be neglected because they probably lie within the error range of the method (Fig. 9b). The percentages of layer-parallel strain estimated for the upper horizons increase progressively up section from somewhat more than -1% to about -6.5%. These values are negative indicating that the current length of the horizons is less than their initial length, i.e., layer-parallel shortening occurred. The average percentage of layer-parallel strain is -2.1 %.

To estimate the bulk strain suffered by the structure we followed a methodology developed by Masini et al. (2010a). This methodology consists of the following steps. a) Placing circular markers in the deformed, geological cross-section. b) Restoring the section together with the markers. c) After restoration, the circular markers become ellipses whose axes ratio (called ellipticity coefficient), accompanied by an algebraic transformation, may be employed as a measure of strain. This ratio ranges from 1 (no deformation) to values close to 0 (strong deformation). d) Obtaining the distribution of the deformation in the deformed section performing an interpolation procedure using as input data the strain values of each marker. In the fault-propagation fold depicted in figure 6a the strain is mainly concentrated in the forelimb, especially in the uppermost beds of the stratigraphic sequence (Fig. 10a), where abundant second order thrust faults and folds occur. The minimum ellipticity coefficient achieved is 0.15. The occurrence of a certain amount of layer-parallel and bulk strain is consistent with the irregular cleavage surfaces identified in the griotte limestones in some portions of the outcrop (Masini et al., 2010a, 2010b).

4.3. Detachment folds

The unit composed of alternations of radiolarites and slates is mainly deformed by two, decimetre to almost metre-scale, anticlines and one syncline in between them (Fig. 6b). These kink-like to rounded, open to close folds are asymmetrical, south-vergent structures, so that the southern limb of the anticlines (forelimb) is short and sub-vertical or even slightly overturned, whereas the northern limb (backlimb) is much longer and dips from sub-horizontal to moderate. The hinge zones and the steep limbs are thickened with respect to the gently dipping limbs; the maximum thickness may reach almost 200 % in hinge zones, although values around 115-125 % are common. Second-order folds, as well as small thrusts repeating beds, folded in some cases, are partly the cause of the thickening. Disharmonies and hinge collapses have been also recognized within these folds. The major anticlines and the syncline are interpreted as detachment folds related to the main detachment level, i.e., the boundary between the radiolarites and slates unit and the underlying griotte limestones unit. Second-order detachment surfaces occur at different horizons within the stratigraphic succession. The folds involving the radiolarites and slates unit might be interpreted as a ductile shear response of southwards motion of the overlying unit formed by alternations of griotte limestones, grey limestone and slates in relation to the underlying griotte limestones unit.

The radiolarites and slates unit lay above the rough top of the underlying griotte limestones unit, folded by the fault-propagation fold developed within the griotte limestones. The radiolarites and slates are approximately parallel to the griotte limestones top towards the south but are oblique to the griotte limestones top towards the north (Fig. 6b). Thus, this surface separates layers in a hangingwall flat situation over a footwall flat towards the north, and in a hangingwall ramp position over a footwall flat towards the south. Since the lowermost portion of the radiolarites and slates succession is missing towards the south, the boundary between the radiolarites and slates and the griotte limestones is partly a subtractive contact. Despite the obliquity between the hangingwall layers and the surface, we call this surface “a detachment” because it separates two mechanical units that exhibit a completely different internal structure. The geometry of the radiolarites and slates just above the detachment may be caused by flow of ductile rocks at the base of the succession during amplification of the detachment folds involving the radiolarites and slates. The area of the inner core of detachment anticlines in whose development intervene the limb rotation mechanism increases extremely in the first stages (Fig. 11) and needs to be filled in with rocks coming from adjacent regions, e.g. adjacent synclines, causing rock flow (e.g., Wiltschko and Chapple, 1977; Homza and Wallace, 1995; Bulnes and Poblet, 1999). If this hypothesis were correct, the amplification of the detachment folds developed within the radiolarites and slates probably stopped when: a) all the available ductile material in adjacent regions had already flowed (Poblet and McClay, 1996), b) the anticline forelimbs reached a sub-vertical dip and the area of the anticline inner core started to decrease (Fig. 11) but the ductile materials could not flow away from the anticline cores because this would require lifting a thick stratigraphic sequence above, or c) the shortening responsible for the development of the detachment folds ended up.

The boundary between the radiolarites and slates unit and the overlying unit formed by alternations of griotte limestones, grey limestones and slates looks like a normal stratigraphic contact in most part of the outcrop, where beds are approximately parallel. However, it corresponds to an upper detachment with respect to the syncline developed in the radiolarites and slates unit in the southern part of the outcrop. Therefore, this contact behaves as a local detachment only at specific points.

To determine the layer-parallel strain caused by the detachment folds we followed the methodology presented in the previous section. The layer-parallel strain was estimated for the southernmost syncline depicted in the geological profile in figure 6b, which is bounded by an upper detachment. The anticlines were not used for the calculations because some folded layers in the inner core of the anticlines are cut by the lower detachment. A lost area diagram was constructed and the amount of shortening estimated (Table 1) (Fig. 9c). The difference between the depth to detachment obtained from the lost area diagram and the actual depth to detachment observed in the field is 3 cm. The small difference between both depths to detachment suggests that the shortening estimate is correct and validates the geological profile from the cross-sectional area point of view. Using equations (1) and (2) we estimated the initial bed length before deformation and the layer-parallel strain. The layer-parallel strain values are negative indicating that the current bed length of the horizons is lesser than the initial one, and therefore, that layer-parallel shortening took place. The percentages are relatively high in the uppermost horizons reaching -26.2 %, decreasing downsection to -4.5% (Fig. 9d). The average percentage is -16.4 %.

To determine the bulk strain caused by the detachment folds we followed the methodology presented in the previous section. The strain obtained is mostly distributed in the hinge zones and in the forelimbs of the detachment folds where the maximum bed thickening occurred (Fig. 10b). The minimum ellipticity coefficient measured is 0.08.

4.4. Fault-bend folds

Almost no structures occur within the alternations of griotte limestones, grey limestones and slates, except for an isolated small fault-bend fold with low displacement developed in a few centimetres thick, grey limestone bed with red slates on top. Most of the fault-bend folds are developed in the overlying grey limestones unit and their main features are described below.

Various grey limestone beds are folded by parallel or almost parallel, smooth anticlines, with rounded geometry and decimetre to metre sizes (Fig. 6c). These folds are asymmetrical and north-vergent, so that the northern limbs (forelimbs) dip gently (from 15° to 25°) and are shorter than the southern limbs (backlimbs) which are sub-horizontal (from 5° to 10°) and longer. Their amplitude is usually smaller than their width. These folds are developed in the hangingwall of thrusts subparallel to bedding, which exhibit some segments of gentle dip to the south. The thrusts are north-directed and are responsible for centimetre to decimetre displacements in cross section view. The beds in contact with these thrusts exhibit hangingwall flats on both footwall flats and ramps, as well as hangingwall ramps on both footwall flats and ramps. The geometrical features of the folds and thrusts, and the different ramp-flat situations of the layers in relation to the thrusts point out that these structures could be interpreted as ramp folds, in particular as fault-bend folds.

In order to check whether the studied structures fit the classical fault-bend fold model (Suppe, 1983), the interlimb angle of one of the fault-bend folds was plotted versus its thrust ramp dip on a specific chart for fault-bend folds (Jamison, 1987) (Fig. 7b). Since the fault-bend folds developed in the upper part of the grey limestones unit are deformed by the ones developed in the lower part of this unit (Fig. 6c), we chose the less deformed structure to carry out the plot, that is the lowermost structure in the geological profile. The data plotted on the graph predict that the structures can be interpreted as fault-bend folds with constant thickness. Thus, the result is satisfactory because the actual example analysed is a parallel fold. Moreover, to ensure this result the displacement on the fault measured for different horizons was plotted versus the distance from each cut-off point to an arbitrary reference point along the fault according to the Chapman and Williams (1984) technique (Fig. 8b). The function obtained for the same fault-bend fold analysed above consists of two segments: a) the lowest constant displacement segment corresponds to beds on a hangingwall flat situation located on the upper detachment, and b) the variable displacement segment corresponds to beds in a hangingwall ramp situation located on the thrust ramp and on the upper detachment. This pattern is in accordance with that of fault-bend folds (e.g., McConnell et al., 1997). According to Hughes and Shaw (2014), a characteristic feature of fault-bend folds is that the ratio of the displacement above the thrust bend to the displacement below the thrust bend (R) predicted by the fault-bend folding theory (Suppe, 1983) minus one is equivalent to the slope of the variable displacement segment. Taking into account the thrust ramp dip and the interlimb angle of the example analysed, the fault-bend fold theory predicts that R is approximately 0.9 for this example. Thus, 0.9 minus 1 equals -0.1 and this value coincides with the slope of the linear best-fit function that fits the data in the variable displacement segment (Fig. 8b). This confirms that the analysed structure corresponds to a fault-bend fold.

To estimate the percentages of layer-parallel strain related to the fault-bend folds we followed the strategy described above (Table 1). We did not calculate the layer-parallel strain for all the folds, bur for the lowermost anticline depicted in the geological profile in figure 6c. The unfolded bed length, the width of the structure, the excess area and the height with respect to a reference level were measured. The lost area diagram using data from this structure supplied the amount of shortening (Fig. 9e). Then, the depth to detachment obtained using the lost area diagram was compared with the actual depth to detachment observed in the field. The difference between the actual depth to detachment and the estimated value is almost 4 cm pointing out that the shortening estimated using the lost area diagram is approximately correct and validating the geological profile from the cross-sectional area point of view. Since the estimated detachment depth is greater than the detachment depth observed in the field (Fig. 9e), the linear best-fit function has a higher slope than it would have if the estimated detachment depth were equal to that observed. This means that the shortening obtained using the best-fit function is somewhat higher than the actual shortening. Finally, the initial bed length before deformation and the amount of layer-parallel strain were obtained employing equations (1) and (2) respectively. The values of layer parallel strain are negative indicating that the current bed length of the horizons is lesser than the initial one. The percentages are low in between -0.8 % and -2.9 % (Fig. 9f) averaging -1.9 %. The percentages of layer-parallel strain estimated for the lower horizons are lower than those estimated for the upper horizons. Since the shortening used to calculate the amount of layer-parallel strain is somewhat greater than the actual shortening, the estimated layer-parallel strain is also somewhat greater than the actual one.

To estimate the bulk strain related to the fault-bend folds we followed the strategy described above. The amount of strain is low (the minimum ellipticity coefficient estimated is 0.42) and it is concentrated in the forelimb of the folds, especially in the upper part of the stratigraphic sequence (Fig. 10c).

4.5. Age and burial depth of the fault propagation fold, detachment folds and fault-bend folds

All the folds and related reverse faults depicted in the rotated geological profiles (Fig. 6) involve the Alba Fm. rocks of lower Carboniferous age (Fig. 2). We proposed above that these contractional structures developed before the Villasecino anticline, when beds were flat-lying, or during the initial stages of tilting of the north limb of the Villasecino anticline as fold-accommodation structures. Since the rocks affected by the studied structures are of Carboniferous age and the Villasecino anticline was developed during the Variscan orogeny of Carboniferous age, this implies that the age of the fault-related folds is Carboniferous. Not all the fault-related folds are strictly simultaneous because the fault-bend folds developed in the upper part of the grey limestones unit are deformed by the ones developed at the bottom of this unit (Fig. 6c), and the basal detachment of the radiolarites and slates unit is folded by the underlying fault-propagation fold developed in the griotte limestones unit (Fig. 6b). Therefore, it seems that deformation propagated from the upper terms of the Alba Fm. rocks downwards.

From a geological section across the study area by Rodríguez-Fernández et al. (1990) (cross section III-III') we estimated that the minimum thickness of the Carboniferous stratigraphic succession involved in Variscan structures above the studied outcrop would have been around 1.5 km (Fig. 1d). However, this may be a minimum depth of burial by the time of formation of the structures. Thus, the sole thrust of the Variscan Somiedo structural unit, which crops out north, south and west of the Villasecino anticline forming a semi-tectonic window (De Sitter, 1962; Marcos, 1968; Martínez-Álvarez et al., 1968; Alonso et al., 1989; Rodríguez-Fernández et al., 1990; Instituto Geológico y Minero de España, 2005-2011) and carrying out a more than 2 km thick Paleozoic succession, is folded by the Villasecino anticline (Alonso et al., 1989; Rodríguez-Fernández et al., 1991) (Fig. 1b). Since the studied outcrop is located in the footwall of the Somiedo sole thrust, the Somiedo thrust sheet could have been also located on top of the Carboniferous succession above the studied outcrop by the time the thrust-related folds were formed. Therefore, if the studied thrust-related folds were developed before the emplacement of the Somiedo thrust sheet, then the burial depth would have been 1.5 km, whereas if they developed after the emplacement of the Somiedo thrust sheet, the burial depth would have been 3.5 km. This range is consistent with the Kübler index of illite (KI) and the conodont colour alteration index (CAI) obtained in this region (García-López et al., 1999, 2007), which indicate that the outcrop is located in a diagenetic, that is, non-metamorphic area.

4.6. Normal faults

In the central portion of the outcrop, we mapped two faults gently inclined, one towards the S and another towards the N that offset the middle-upper part of the radiolarites and slates unit, the unit formed by griotte limestones, grey limestones and slates, and the lower part of the grey limestones unit (central-lower portion of Fig. 3). The offset caused by these metre-scale faults is reverse and reaches up to some decimetres. Smaller faults with similar characteristics have been recognized as well. Once the geological interpretation of the outcrop is rotated in a clockwise sense looking ESE around a horizontal ESE–WNW axis, these two main faults become conjugate normal faults with a steep dip towards the N and towards the S defining a small graben (left portion of geological profile depicted in Fig. 4b). The displacement along these normal faults decreases down-section to zero within the radiolarites and slates unit where both faults join. Up-section, the southernmost normal fault is offset by a thrust developed within the grey limestones unit (right portion of geological profile depicted in Fig. 6c). The facts that: a) these faults involve Carboniferous rocks; b) their geometry, displacement and structural relationships makes sense once the geological interpretation is rotated, pointing out that they developed before the tilting of the north limb of the Villasecino anticline; and c) they developed prior to the thrust-related folds present in the outcrop, suggest that they may be interpreted as an evidence of a possible extensional event of Early Carboniferous age previous to the Variscan orogeny.

4.7. Oblique faults

A few decimetre to metre-scale faults with relatively gentle dip towards the WNW have been recognized in different parts of the outcrop. The slickenfibres developed on the fault surfaces usually exhibit a NW-SE trend regardless of the orientation of the faults indicating that the hangingwall moved towards the SE. They are oblique faults with a dip-slip (reverse) component and a subordinate strike-slip (left-lateral) one. The geometry and displacement along these faults does not seem to make sense once the geological interpretation is rotated in a clockwise sense looking ESE around a horizontal ESE–WNW axis. Moreover, these faults seem to cut and offset some thrusts present in the outcrop. This suggests that these oblique faults developed after thrusting and after tilting of the north limb of the Villasecino anticline.

The normal faults described above display oblique NW-SE slickenfibres on their surfaces indicating that the hangingwall moved towards the SE. The displacement along these normal faults, deduced by correlating beds on both fault blocks, is not consistent with the one they should have according to these slickenfibres. This suggests that these faults were originally normal faults later on reactivated as oblique faults.

Hectometre to kilometre-scale faults, with a similar motion to that of the oblique faults described, have been mapped in surrounding areas (see for instance geological maps by Rodríguez-Fernández et al., 1990 and Instituto Geológico y Minero de España, 2005-2011, and Fig. 1c). In these geological maps NW-SE faults with apparent left-lateral motion and NE-SW faults with apparent right-lateral motion offset the Villasecino anticline trace. The NW-SE and NE-SW sets could be interpreted as a conjugate fault system. If this were correct, these two fault families could result from approximately N-S shortening and may be related to the final stages of development of the Villasecino anticline, to the closure of the Ibero-Armorican Arc and/or to the Alpine contraction. Thus, a) the E -W trending Villasecino anticline may have been caused by local N-S shortening assuming that the shortening responsible for its formation was approximately perpendicular to the fold trend, b) some authors attributed the formation of the Ibero-Armorican Arc to a late Paleozoic N-S shortening that bent an initial nearly linear Variscan belt (Julivert, 1971b; Julivert and Marcos, 1973; Stewart, 1995 amongst others), and c) analysis of fault populations in Mesozoic rocks north of the study area yielded an approximately N-S shortening direction during the Cenozoic Alpine contraction (Lepvrier and Martínez-García, 1990; Uzkeda et al., 2016).

5. CONTROLS ON DEVELOPMENT OF FAULT-BEND, FAULT PROPAGATION AND DETACHMENT FOLDS

A large number of parameters may exert a control to a certain extent on the development of a specific fold/thrust style: mechanical stratigraphy (single layers or multilayers, strength, thickness of the cover and ductile layers, shear strength of layer interfaces, dominant members, stacking of lithologic types, weakness of the décollement layer, anisotropy, etc.), confining pressure, pore pressure, temperature, strain rate, stress state, amount of shortening, syn-tectonic sedimentation, etc. (e.g., Chester et al., 1991; Dixon and Liu, 1992; Jamison, 1992; Liu and Dixon, 1995; Erickson, 1996; Stewart, 1996; Storti et al., 1997; Chester, 2003; Albertz and Lingrey, 2012; Hughes et al., 2014; Yan et al., 2016; Li and Mitra, 2017). All the fault-related folds described in the studied outcrop developed in the same structural position, so that the average dip of the beds, the age of the structures and the pressure and temperature conditions when they formed were basically the same. Unfortunately, the outcrop dimensions are limited, and therefore, we cannot check whether the shortening suffered by the different mechanical units was the same or it was different. However, it is likely that all of them have undergone similar amounts of shortening accommodated in different manners. Thus, the main differences between the zones in which fault-bend, fault-propagation or detachment folds developed are: 1) the depth at which they were formed, and 2) the rheological and some stratigraphic features of the rocks involved in the structures. In relation to the depth, it seems unreasonable that a difference of a few meters could be responsible for the formation of different types of fault-related folds. Therefore, we conclude that, at least in this particular case, the development of one or another type of fault-related fold was essentially controlled by the mechanical stratigraphy (Fig. 12).

Some features of the structures developed in each mechanical unit supply information about the behaviour of the unit. Figures 12 and 13 illustrate the layer-parallel and bulk strain, the forelimb dip, the supplementary angle of the interlimb angle, and the forelimb and hinge thickening in the fault-propagation fold involving the griotte limestones unit, a detachment fold involving the radiolarites and slates unit, and a fault-bend fold affecting the grey limestones unit. Regardless of the type of fold/thrust interaction, all show forelimb thickening accompanied by a certain amount of strain. The ramp folds (fault-bend and fault-propagation folds) do not show thickening or strain in the hinge area, while the detachment folds do. The fault-bend fold shows the lowest values for all parameters, the fault-propagation fold shows intermediate values, and the detachment fold shows the highest values. These figures suggest that the lowest deformation occurred in fault-bend folds, intermediate in fault-propagation folds and the greatest deformation occurred in detachment folds. These data are in accordance with the fact that the grey limestones unit is the most competent unit, followed by the griotte limestones unit, whereas the radiolarites and slates unit is the most incompetent one.

The mechanical stratigraphy exerted a strong control on the position of the detachments within the stratigraphic succession. Detachments are located where abrupt changes take place in all the different properties of the rocks located above and below the boundary (see the logs in Fig. 12 and the graph in Fig. 2c). The lowermost detachment is located within the black slates of the Vegamián Fm. below the griotte limestones unit, and the uppermost one between the griotte limestones unit and the unit formed by radiolarites and slates. Local, second-order detachments may develop at those boundaries within the stratigraphic succession where the changes in the rock mechanical properties are significant but not dramatic, such as the boundary between the radiolarites and slates unit and the unit made up of griotte limestones, grey limestones and slates (Figs. 2 and 12). Detachments do not occur at those boundaries where the changes between the rock mechanical properties are minor, such as the boundary between the unit formed by griotte limestones, grey limestones and slates and the overlying grey limestones unit (Figs. 2 and 12). These detachments are necessary to allow different types of thrust-related folds with different vergence and dimensions to be generated at different levels of the stratigraphic succession. Thus, the structures recognized at a certain depth domain cannot be extrapolated to the whole succession.

The dimensions of the fault-related folds mapped in the outcrop may be influenced by the mechanical stratigraphy as well. The graph in figure 14, based on outcrop observations, illustrates the relationship between the dimensions of the structures and three characteristics of the mechanical units: presence/absence of a basal detachment, lithological monotony/alternation of lithologies of different competence, and smoothness/roughness of the bedding surfaces. The most important discontinuity in the griotte limestones unit lies at its base, when it comes into contact with the dark slates of the Vegamián Fm. through a detachment. The internal discontinuities within the griotte limestones unit are the bedding surfaces, but there are no significant changes in the features of the different griotte limestone strata. In addition, the bedding surfaces within the griotte limestones are rough making sliding between layers difficult. The basal detachment and absence of internal mechanical contrasts/discontinuities caused that the whole unit acted as solidary set, and therefore, a large-scale, single tectonic structure developed. As in the case of griotte limestones unit, the most important discontinuity in the radiolarites and slates unit lies at the base of the unit, when it comes into contact with the griotte limestones through a detachment. Unlike the griotte limestones unit, the radiolarites and slates unit involves alternations of lithologies. Each bedding surface separating a radiolarite layer from a slate layer is a significant internal discontinuity because of the different mechanical properties of these two lithologies. In addition, bedding surfaces are smooth allowing beds to slide between them easily. The occurrence of an important detachment forced the radiolarites and slates unit to behave as a solidary set (large-scale detachment folds that affect almost the whole unit). However, the existence of internal, efficient discontinuities and mechanical contrasts led to development of various minor, second-order structures within the unit. The most important difference between the grey limestones unit and both the griotte limestones unit and the slates and radiolarites unit is the absence of a significant detachment at its base; the radiolarites and slates unit passes gradually onto the grey limestones unit. Thus, the shortening suffered by the grey limestones unit could not be accommodated primarily along a basal detachment, and therefore, it sought other discontinuities capable of accommodating it. The most important discontinuities within the grey limestones unit are the bedding surfaces, which include some interbedded slates and are smooth allowing easy sliding between beds. As the grey limestones unit does not have a basal detachment but internal discontinuities, it shortened though small-scale structures that involved only certain layers. Regarding the unit composed of griotte limestones, grey limestones and slates, the absence of a basal detachment, the presence of lithologies of different competence and the presence of both rough and smooth bedding surfaces led to virtually no development of structures.

Ramp folds, i.e., fault-bend folds and fault-propagation folds, are developed in thick-bedded, monotonous successions of relatively strong, brittle rocks (limestones), whereas detachment folds involve thin-bedded alternations of strong and weak rocks, which constitute a relatively ductile unit (alternations of radiolarites and slates) (Fig. 2 and 12). In accordance with Chester et al. (1991) amongst others, these observations confirm that shortening in isotropic, competent lithologies primarily involve faulting, whereas thinly layered, anisotropic units (alternations of competent and incompetent materials) shorten mainly by folding. The mechanical units analysed were subjected to a flexural slip mechanism, and this means that the threshold above which these bedding surfaces act as shear surfaces was exceeded. The easiness or difficulty to slide of the bedding surfaces is probably related to the morphology of the bedding surfaces, which may have influenced to a certain extent the type of fold/thrust style developed. Thus, boundaries between layers in the radiolarites and slates unit and in the grey limestones unit are frictionless or exhibit a low friction because they are generally smooth, and therefore, they are free or almost free to slip. In contrast, boundaries between griotte limestone layers are partially bonded because they are rough, and therefore, they exhibit high shear strength. In the grey limestones unit, the frictional shear strength between bedding surfaces was low and this is the reason why thrusts developed mainly along bedding surfaces forming flats and short ramps across one, or more than one, layer. Motion along these curved, staircase thrust surfaces caused fault-bend folding. In the griotte limestones unit, the lowest frictional resistance to shear occurred in the underlying black slates, and this explains why the main thrust (detachment) developed within these rocks. When the thrust ramped up across the griotte limestone layers, it did not run along bedding surfaces but cut across them, probably because the frictional resistance of these surfaces was low enough to allow these surfaces to accommodate layer-parallel shear but not low enough to allow the thrust to run along them. On the other hand, as the hangingwall translated up the ramp, shortening was accommodated through hangingwall folding and thrust propagation, as well as second order folding and faulting near the fault tip, causing fault-propagation folding. In the radiolarites and slates unit, while bedding surfaces are smooth and have a low frictional resistance to sliding, the boundary between the radiolarites and slates unit and the underlying griotte limestones unit has an even lower frictional resistance to sliding, causing the main detachment. Some particular ductile beds within the succession have an extremely low strength leading to second-order detachment and thrusting. Consequently, shortening was accommodated by detachment folding. Figure 15 illustrates a triangular graph to show the main stratigraphic and rheologic features that control the formation of the different types of fault-related folds in the studied outcrop.

The graphs in figures 14 and 15 can be used to predict the size and/or types of fault-related folds expected in a stratigraphic sequence of known characteristics, such as in a case where only the superficial portion of the structures crop out and no subsurface data are available. The graphs can also be used in a reverse way, that is, to determine the characteristics of a stratigraphic sequence when the size and/or type of the structures are known. For example, this would be the case of subsurface fault-related folds mapped on seismic data, involving a stratigraphic sequence of unknown features because it does not crop out and no wells through it are available. When plotting the characteristics of a stratigraphic succession on the triangular diagrams, it could happen that the obtained points fall in between the vertices of the triangle. Lets us imagine an example in which the plotted points fall between fault-bend folds and fault-propagation folds, but closer to fault-bend folds. This would mean either that the types of fault-related folds expected are hybrid structures, i.e., transported fault-propagation folds, or that fault-bend folds predominate over fault-propagation folds in the study area.

6. CONCLUSIONS

Mechanical stratigraphy was the main control on the occurrence of fault-bend, fault-propagation and detachment folds developed under diagenetic conditions, at an approximate burial depth of 1.5 to 3.5 km, in an homoclinal succession located in the limb of a kilometre-scale, tight anticline formed during Carboniferous times in the Cantabrian Zone (foreland fold and thrust belt of the Variscan orogen in NW Iberian Peninsula). Thus, fault-bend folds developed in grey limestones, fault-propagation folds developed in red, nodular (griotte) limestones, and detachment folds developed in alternations of radiolarites and slates. The greatest amount of layer-parallel and bulk strain, forelimb dip and forelimb/hinge thickening, and the smallest interlimb angle, took place in detachment folds. The lowest values occurred in fault-bend folds and intermediate values in fault-propagation folds. All these fault-related folds show some strain in the forelimb, although only the detachment folds exhibit thickening and strain in the hinge area. Since these mechanical units are arranged one above the other in a normal stratigraphic order, this caused a change in the structural style at depth. Ramp folds developed in thick-bedded, isotropic, competent units, whereas detachment folds developed in thin-bedded, anisotropic, incompetent units. More competent rocks and smooth bedding surfaces favoured the development of fault-bend folds, whereas less competent and rough bedding surfaces led to fault-propagation folding. The main detachments are located at the boundaries between the griotte limestones unit and underlying black slates, and between the griotte limestones unit and the radiolarites and slates unit, i.e., between mechanical units with notable changes in their mechanical properties (grain size, percentage of incompetent rocks, erosion resistance, bed thickness and bedding roughness). The structures developed in griotte limestones are larger-scale structures that involve the entire unit, because it has a basal detachment and is a monotonous sequence with high friction, rough bedding surfaces. On the contrary, the structures developed in the grey limestones are small-scale structures that only involve some layers, since this unit does not have a basal detachment and is a monotonous sequence with low friction, smooth bedding surfaces. Both larger-scale structures, that involve the whole unit, and small-scale structures, that only involve some layers, coexist in the radiolarites and slates unit because this unit has a basal detachment and consists of alternations of lithologies of different competence with smooth bedding surfaces that act as "internal detachments".

The study carried out here indicates that mechanical stratigraphy exerts a strong influence in fold/thrust interactions, as well as in detachment positions and in the size of the structures. These points are key issues not only in the usual structural geology and mapping research tasks carried out at academia, but also in the hydrocarbon industry prior to drilling structural traps. For instance, proper identification of the fold/thrust style is essential because distinct classes of structures often have different trap geometries, hydrocarbon charge paths and reservoir strain characteristics. Correct diagnosis of fold/thrust styles is also essential in geological/geophysical surveys in charge of assessing seismic hazard, since fault slip rates of seismically-active, blind thrusts are generally inferred from patterns of uplift above fault-related folds, and different types of structures exhibit different relations between fault slip and uplift.

In regions involving heterogeneous stratigraphic sequences, geologists cannot rely solely on the use of surface data to reconstruct the structures at depth because the outcropping structures may not be appropriate analogues for subsurface structures.

Thus, when constructing geological cross-sections and/or 3D models to accurately predict the geometry and relationships between the structures, a thorough understanding of the stratigraphic facies realms and their features, based on lithological information from surface outcrops, geophysical data and/or wells, is crucial. This would allow understanding the role of the mechanical stratigraphy, and therefore, may help reducing uncertainties in deciding which fold/thrust model is more appropriate to apply in the interpretation of a given structure, specially in those regions with scarce, relatively poor or irregularly distributed available subsurface data.

Although we believe the approach presented here is one more step in the understanding of the causes that influence fold/thrust interaction, it should be noted that: 1) the example studied is a small-scale case with particular types of rocks, and 2) we cannot rule out that, rather than the mechanical stratigraphy, other factors such as pressure, temperature, strain rate, stress state, amount of shortening, syn-tectonic sedimentation, etc. may be controlling factors of the type of fold/thrust interaction in other regions. Therefore, this approach should be used as an additional guideline to support other structural techniques.

ACKNOWLEDGEMENTS

We would like to acknowledge financial support by research project CGL2015-66997-R (“Aplicación del análisis del plegamiento a la investigación de recursos geológicos” -AAPLIREGE-) funded by the Spanish Ministry for Economy and Competitivity and the European Fund for Regional Development (FEDER). H. Uzkeda work has been partly supported by research contract CN-16-014 (“Convenio específico para la realización de un trabajo de investigación post-doctoral en la disciplina de Geología”) and I. Rodríguez-Álvarez work has been partly supported by research contract CN-016-15 ("Convenio específico para la realización de una tesis doctoral en la línea de investigación en Geología y Geosistemas del programa de doctorado en Biogeociencias"), both under the framework agreement between Repsol Exploración S.A. and the University of Oviedo. We thank Midland Valley for permission to use the software Move (Academic site software license and support agreement number 1915). Richard Allmendinger and Nestor Cardozo are thanked for permission to use their software Stereonet. We thank the editor I. Alsop, J.L. Alonso, M. Masini, F. Bastida, L.P. Fernández and an anonymous reviewer for their scientific contribution, J.G. Antuña for maintaining the software for structural interpretation and modelling, and I. Moriano for assisting us during one field campaign.

REFERENCES

Albertz, M., Lingrey, S., 2012. Critical state finite element models of contractional fault-related folding: Part 1. Structural analysis. Tectonophysics 576, 133-149.

Aller, J., Álvarez-Marrón, J., Bastida, F., Bulnes, M., Heredia, N., Marcos, A., Pérez-Estaún, A., Pulgar, F.J.A., Rodríguez-Fernández, R., 2004. Estructura, deformación y metamorfismo (Zona Cantábrica). In: Vera, J.A. (Ed.), Geología de España. Sociedad Geológica de España-Instituto Geológico y Minero de España, Madrid, 42–49.

Allmendinger, R. W., 1998. Inverse and forward numerical modeling of trishear fault-propagation folds. Tectonics 17(4), 640-656.

Alonso, J. L., Aller, J., Bastida, F., Marcos, A., Marquínez, J., Pérez-Estaún, A., Pulgar, J. A., 1991. Memoria del mapa Geológico de España. Escala 1:200.000. Hoja 2 (3-1) Avilés. Instituto Tecnológico GeoMinero de España, Madrid.

Alonso, J. L., Álvarez-Marrón, J., Pulgar, J. A., 1989. Síntesis cartográfica de la parte sudoccidental de la Zona Cantábrica. Trabajos de Geología 18, 145-155.

Alonso, J. L., García-Alcalde, J. L., Aramburu, C., García-Ramos, J. C., Suárez, A., Abad, I. M., 2008. Sobre la presencia de la Formación Naranco (Devónico Medio) en el Manto de Bodón (Zona Cantábrica): implicaciones paleogeográficas. Trabajos de Geología 28, 159-169.

Alonso, J. L., Pulgar, F. J., García-Ramos, J. C., Barba, P., 1996. Tertiary basins and Alpine tectonics in the Cantabrian Mountains. In: Friend, P.F., Dabrio, C.J. (Eds.), Tertiary basins of Spain: The stratigraphic record of crustal kinematics. Cambridge University Press, Cambridge, 214-227.

Alonso, J. L., Marcos, A., Suárez-Rodríguez, A., 2009. Paleogeographic inversion resulting from large out of sequence breaching thrusts: the León Fault (Cantabrian Zone, NW Iberia). A new picture of the external Variscan thrust belt in the Ibero-Armorican Arc. Geologica Acta 7(4), 451-473.

Anastasio, D. J., Erslev, E. A., Fisher, D. M., Evans, J. P. (Eds.), 1997. Fault-related folding. Journal of Structural Geology 19(3-4).

Barrois, C., 1882. Recherches sur les terrains anciens des Asturies et de la Galice. Memoires de la Société Géologique du Nord 2(1), 1-630.

Brandes C., Tanner, D. C., 2014. Fault-related folding: A review of kinematic models and their application. Earth-Science Reviews 138, 352–370.

Bulnes, M., Aller, J., 2002. Three-dimensional geometry of large-scale fault-propagation folds in the Cantabrian Zone, NW Iberian Peninsula. Journal of Structural Geology 24, 827-846.

Bulnes, M., Poblet, J., 1999. Estimating the detachment depth in cross sections involving detachment folds. Geological Magazine 136, 395-412.

Chamberlin, R. T., 1910. The Appalachian folds of central Pennsylvania. Journal of Geology 18, 228-251.

Chapman, T., Williams, G., 1984. Displacement-distance methods in the analysis of fold-thrust structures and linked-fault systems. Journal of the Geological Society 141(1), 121-128.

Chester, J. S., 2003. Mechanical stratigraphy and fault–fold interaction, Absaroka thrust sheet, Salt River Range, Wyoming. Journal of Structural Geology 25, 1171–1192.

Chester, J. S., Logan, J. M., Spang, J. H., 1991. Influence of layering and boundary conditions on fault-bend and fault-propagation folding. Geological Society of America Bulletin 103(8), 1059-1072.

Comte, P., 1959. Recerches sur les terrains anciens de la Cordillère Cantabrique. Memorias del Instituto Geológico y Minero de España 60.

Currie, J. B., Patnode, H. W., Trump, R. P., 1962. Development of folds in sedimentary strata. Geological Society of America Bulletin 73, 655–674.

Dahlstrom, C. D. A., 1970. Structural geology in the eastern margin of the Canadian Rocky Mountains. Bulletin of Canadian Petroleum Geology 18(3), 312-406.

De Sitter, L.U., 1962. The structure of the southern slope of the Cantabrian Mountains. Geological map with section scale 1:100,000. Leidse Geologische Medelelingen 26, 255–264.

Dixon, J. M., Liu, S., 1992. Centrifuge modelling of the propagation of thrust faults. In: McClay, K. (Ed.), Thrust tectonics. Chapman and Hall, London, 53-69.

Epard, J. L., Groshong Jr, R. H., 1993. Excess area and depth to detachment. AAPG Bulletin 77(8), 1291-1302.

Erickson, S. G., 1996. Influence of mechanical stratigraphy on folding vs faulting. Journal of Structural Geology 18(4), 443-450.

Erslev, E. A., 1991. Trishear fault-propagation folding. Geology 19(6), 617-620.

García-López, S., Bastida, F., Brime, C., Aller, J., Valín, M. L., Sanz-López, J., Méndez, C. A., Menéndez-Álvarez, J. R., 1999. Los episodios metamórficos de la Zona Cantábrica y su contexto estructural. Trabajos de Geología 21, 177-189.

García-López, S., Brime, C., Valín, M. L., Sanz-López, J., Bastida, F., Aller, J., Blanco-Ferrera, S., 2007. Tectonothermal evolution of a foreland fold and thrust belt: the Cantabrian Zone (Iberian Variscan belt, NW Spain). Terra Nova 19(6), 469-475.

Ginkel, A. C. van, 1965. Carboniferous fusulinids from the Cantabrian Mountains (Spain). Leidse Geologische Medelelingen 34, 1-225.

Groshong Jr, R. H., 2015. Quality control and risk assessment of seismic profiles using area-depth-strain analysis. Interpretation 3(4), SAA1-SAA15.

Groshong, R. H., Jr., Epard, J.-L., 1994. The role of strain in area-constant detachment folding. Journal of Structural Geology 16, 613-618.

Hardy, S., Poblet, J., 1994. Geometric and numerical model of progressive limb rotation in detachment folds. Geology 22, 371-374.

Homza, T. X., Wallace, W. K., 1995. Geometric and kinematic models for detachment folds with fixed and variable detachment depths. Journal of Structural Geology 17(4), 575-588.

Hughes, A. N., Shaw, J. H., 2014. Fault displacement-distance relationships as indicators of contractional fault-related folding style. AAPG Bulletin 98(2), 227-251.

Hughes, A. N., Benesh, N. P., Shaw, J. H., 2014. Factors that control the development of fault-bend versus fault-propagation folds: Insights from mechanical models based on the discrete element method (DEM). Journal of Structural Geology 68, 121-141.

Instituto Geológico y Minero de España, 2005-2011. Mapa geológico continuo de España 1:50.000 (Plan Geode). http://www.igme.es

Jamison, W. R., 1987. Geometric analysis of fold development in overthrust terranes. Journal of Structural Geology 9(2), 207-219.

Jamison, W. R., 1992. Stress controls on fold thrust style. In McClay, K. R. (Ed.), Thrust tectonics. Chapman, Hall, London: 155-164.

Julivert, M., 1971a. Décollement tectonics in the Hercynian Cordillera of NW Spain. American Journal of Science 270, 1–29.

Julivert, M., 1971b. L'évolution structurale de l'arc asturien. In: Histoire structurale du Golfe de Gascogne, Technip Editions, Paris 1, 1-28.

Julivert, M., 1979. A cross-section though the northern part of the Iberian Massif: its position within the Hercynian fold belt. Krystalinikum 14, 51–67.

Julivert, M., 1981. A cross-section though the northern part of the Iberian Massif. Geologie en Minbouw 60, 107–128.

Julivert, M., 1983. La estructura de la Zona Cantábrica. In: Comba, J.A. (Ed.), Geología de España. Libro Jubilar, J.M. Ríos, Tomo I. Instituto Geológico y Minero de España, Madrid, 339–381.

Julivert, M., Arboleya, M. L., 1984. A geometrical and kinematical approach to the nappe structure in an arcuate fold belt: the Cantabrian nappes (Hercynian chain, NW Spain). Journal of Structural Geology 6, 499-519.

Julivert, M., Marcos A., 1973. Superimposed folding under flexural conditions in the Cantabrian Zone (Hercynian Cordillera, northwestern Spain). American Journal of Science 273, 353-375.

Lepvrier, C., Martínez-García, E., 1990. Fault development and stress evolution of the post-Hercynian Asturian basin (Asturias and Cantabria, northwestern Spain). Tectonophysics 184, 345-356.

Li, J., Mitra, S., 2017. Geometry and evolution of fold-thrust structures at the boundaries between frictional and ductile detachments. Marine and Petroleum Geology 85, 16-34.

Lisle, R., Poblet, J., 2010. Preface: structural analysis of fold-and-thust belts. Geological Journal 45(5-6), 487-488.

Liu, S., Dixon, J. M., 1995. Localization of duplex thrust-ramps by buckling: analog and numerical modelling. Journal of Structural Geology 17(6), 875-886.

Marcos, A., 1968. La tectónica de la Unidad de La Sobia-Bodón. Trabajos de Geología 2, 59–87.

Martínez-Álvarez, J. A., Gutiérrez-Claverol, M., Vargas-Alonso, I., 1968. Esquema geológico de la zona de la Cordillera Cantábrica comprendida entre los Puertos ‘‘Pajares’’ y ‘‘Ventana’’ (Asturias-León). Cátedra de Geología, Escuela de Minas de Oviedo, Oviedo.

Masini, M., Bulnes, M., Poblet, J., 2010a. Cross-section restoration: a tool to simulate deformation. Application to a fault-propagation fold from the Cantabrian fold and thrust belt, NW Iberian Peninsula. Journal of Structural Geology 32, 172-183.

Masini, M., Poblet, J., Bulnes, M., 2010b. Structural analysis and deformation architecture of a fault-propagation fold in the southern Cantabrian Mountains, NW Iberian Peninsula. Trabajos de Geología 30, 55-62.

McClay, K.R., 1992. Thrust tectonics: an introduction. In: McClay, K.R. (Ed.), Thrust tectonics. Chapman & Hall, London.

McClay, K. R., 2004. Thrust tectonics and hydrocarbon systems; introduction. In: McClay, K. R. (Ed.), Thrust tectonics and hydrocarbon systems. AAPG Memoir 82, ix-xx.

McClay, K., 2011. Introduction to thrust fault-related folding. In: McClay, K., Shaw, J.H., Suppe, J. (Eds.), Thrust fault-related folding. AAPG Memoir 94, 1-19.

McConnell, D. A., Kattenhorn, S. A., Benner, L. M., 1997. Distribution of fault slip in outcrop-scale fault-related folds, Appalachian Mountains. Journal of Structural Geology 19(3), 257-267.

Mitra, S., Fisher, G. W., 1992. Introduction. In: Mitra, S., Fisher, G. W. (Eds.), Structural geology of fold and thrust belts. Johns Hopkins University Press, The Johns Hopkins Studies in Earth and Space Sciences, Baltimore, ix-x.

Nemcok, M., Schamel, S., Gayer, R., 2009. Thrustbelts: structural architecture, thermal regimes and petroleum systems. Cambridge University Press, Cambridge, 541 p.

Pérez-Estaún, A., Bastida, F., 1990. Cantabrian Zone: structure. In: Dallmeyer, R.D., Martínez-García, E. (Eds.), Pre-Mesozoic Geology of Iberia. Springer-Verlag, Berlin, 55–69.

Pérez-Estaún, A., Bastida, F., Alonso, J. L., Marquínez, J., Aller, J., Álvarez-Marrón, J., Marcos, A., Pulgar, J. A., 1988. A thin-skinned tectonics model for an arcuate fold and thrust belt: the Cantabrian Zone (Variscan Ibero-Armorican Arc). Tectonics 7, 517–537.

Poblet, J., 2004. Geometría y cinemática de pliegues relacionados con cabalgamientos. Trabajos de Geología 24, 127-147.

Poblet, J, Lisle, R., 2011. Kinematic evolution and structural styles of fold-and-thrust belts. In: Poblet, J., Lisle, R. (Eds.), Kinematic evolution and structural styles of fold-and-thrust belts. Geological Society Special Publication 349, 1-24.

Poblet, J., McClay, K., 1996. Geometry and kinematics of single-layer detachment folds. AAPG Bulletin 80(7), 1085-1109.

Poblet, J., Bulnes, M., McClay, K., Hardy, S., 2004. Plots of crestal structural relief and fold area versus shortening: a graphical technique to unravel the kinematics of thrust-related folds. In: McClay (Ed.), Thrust tectonics and hydrocarbon systems. AAPG Memoir 82, 372-399.

Prado, C. de, Verneuil, E. de, 1850. Sur les terrains de Sabero et des environs dans les montagnes de León (Espagne). Bulletin de la Société Géologique de France, 2éme. Série VII, 137-155.

Pulgar, J. A., Alonso, J. L., Espina, R. G., Marín, J. A., 1999. La deformación alpina en el basamento varisco de la Zona Cantábrica. Trabajos de Geología 21, 283-294.

Ramsay, J. G., Huber, M. I., 1987. The techniques of modern structural geology. Volume 2: folds and fractures. Academic Press, London.

Rich, J. L., 1934. Mechanics of low-angle overthrust faulting as illustrated by the Cumberland thrust block, Virginia, Kentucky, and Tennessee. AAPG Bulletin 18, 1584-1596.

Rodríguez-Fernández, L. R., Suárez-Rodríguez, A., Toyos, J. M., López-Díaz, F., Heredia, N., Gutiérrez-Alonso, G., 1990. Mapa geológico de España. Escala 1:50.000. Hoja: 102 (12–7) Los Barrios de Luna. Instituto Tecnológico GeoMinero de España, Madrid.

Rodríguez-Fernández, L. R., Barba, P., Fernández, L. P., Bardají, T., Silva, P. G., Suárez Rodríguez, A., Heredia, N., Gallastegui, G., Paniagua, A., Galán, L., Martínez-Álvarez, J. A., Torres Alonso, M., Gutiérrez Claverol, M., López Díaz, F., Toyos, J. M., Villa, E., Salvador González, C., Bravo Fernández, I., 1991. Memoria del mapa geológico de España. Escala 1:50.000. Hoja: 102 (12–7) Los Barrios de Luna. Instituto Tecnológico GeoMinero de España, Madrid.

Roeder, D., Gilbert, E., Witherspoon, W., 1978. Evolution of macroscopic structure of Valley and Ridge thrust belt, Tennessee and Virginia. Studies in Geology, Department of Geological Sciences, University of Tennesse 2, 1–25.

Savage, J. F., 1979. The Hercynian orogeny in the Cantabrian mountains, Northern Spain. Krystalinikum 14, 91–108.

Savage, J. F., 1981. Geotectonic cross-section through the Cantabrian mountains, northern Spain. Geologie en Mijnbouw 81, 3–5.

Shaw, J. H., Connors, C. D., Suppe, J., 2005. Part 1: structural interpretation methods. In: Shaw, J. H., Connors, C. D., Suppe, J. (Eds.), Seismic interpretation of contractional fault-related folds: an AAPG seismic atlas. American Association of Petroleum Geologists, Studies in Geology 53, 1-58.

Soler, M., 1967. Evolución longitudinal del cabalgamiento de Peña Sobia (Asturias). Acta Geológica Hispánica 2(4), 82-84.

Stewart, S. A., 1995. Paleomagnetic analysis of fold kinematics and implications for geological models of the Cantabrian-Asturian arc, north Spain. Journal of Geophysical Research 100, 20079-20094.

Stewart, S. A., 1996. Influence of detachment layer thickness on style of thin-skinned shortening. Journal of Structural Geology 18(10), 1271-1274.

Storti, F., Salvini, F., McClay, K., 1997. Fault-related folding in sandbox analogue models of thrust wedges. Journal of Structural Geology 19(3), 583-602.

Suess, E., 1892. Das Antlitz der Erde. F. Tempsky, Wien.

Suppe, J., 1983. Geometry and kinematics of fault-bend folding. American Journal of Science 283(7), 684-721.

Suppe, J., 1985. Principles of structural geology. Prentice Hall, New Jersey.

Suppe, J., Medwedeff, D. A., 1990. Geometry and kinematics of fault-propagation folding. Eclogae Geologicae Helvetiae 83(3), 409-454.

Uzkeda, H., Bulnes, M., Poblet, J., García-Ramos, J. C., Piñuela, L., 2016. Jurassic extension and Cenozoic inversion tectonics in the Asturian Basin, NW Iberian Peninsula: 3D structural model and kinematic evolution. Journal of Structural Geology 90, 157-176.

Wagner, R. H., Winkler Prins, C. J., Riding, R. E., 1971. Lithostratigraphic units of the lower part of the Carboniferous in northern León, Spain. Trabajos de Geología 4, 603-663.

Wilkerson, M. S., Wilson, J. M., Poblet, J., Fischer, M. P., 2004. DETACH: an Excel spreadsheet to simulate 2-D cross sections of detachment folds. Computers & Geosciences 30(9), 1069-1077.

Wiltschko, D. V., Chapple, W. M., 1977. Flow of weak rocks in Appalachian Plateau folds. AAPG Bulletin 61(5), 653-670.

Winkler Prins, C. J., 1968. Carboniferous Productidina and Chonetidina of the Cantabrian Mountains (NW Spain): systematics, stratigraphy and paleoecology. Leidse Geologische Medelelingen 43, 41-126.

Yan, D. P., Xu, Y. B., Dong, Z. B., Qiu, L., Zhang, S., Wells, M., 2016. Fault-related fold styles and progressions in fold-thrust belts: Insights from sandbox modeling. Journal of Geophysical Research: Solid Earth, 10.1002/2015JB012397.

FIGURE CAPTIONS

Figure 1: a) Structural sketch of the Cantabrian Zone, b) structural sketch of a portion of the Somiedo-Correcillas and Sobia-Bodón structural units (modified from Rodríguez-Fernández et al., 1990), c) geological map of the region around the studied outcrop (data from Rodríguez-Fernández et al., 1990 and Alonso et al., 2008) with location of cross section line A-A', and d) geological section A–A' across the Villasecino anticline (modified from Masini et al., 2010a).

Figure 2: a) Panoramic photograph of the studied outcrop displaying the stratigraphic units. b) Stratigraphic column of the studied outcrop showing the rock main features used to define the different mechanical units. The percentage of competent rocks has been estimated assuming that limestones and radiolarites are competent rocks, whereas slates are incompetent rocks. c) Pentagonal diagram relating different properties of each mechanical unit. The values of these properties have been extracted from the logs depicted in the stratigraphic column in b).

Figure 3: a) Photo-geological interpretation of the studied outcrop, and b) geological cross-section of the studied outcrop displaying the stratigraphic and mechanical units as well as the main structures.

Figure 4: a) Conceptual geological cross-section showing the location of the studied outcrop within the Villasecino anticline, and b) geological cross-section of the studied outcrop rotated as a rigid body in a clockwise sense looking ESE around the Villasecino anticline fold axis.

Figure 5: Equal area projections in the lower hemisphere using the software Stereonet of measurements of: a) bedding and a fold axis collected in the griotte limestones unit, b) bedding and fold axes collected in the radiolarites and slates unit, c) bedding and fold axes collected in the grey limestones unit, and d) thrust surfaces and related kinematic indicators (striae and slickenfibres). Bedding and thrust surfaces are represented by lines, and fold axes and kinematic indicators as dots.

Figure 6: Geological profiles rotated in a clockwise sense showing the structures developed in: a) the griotte limestones unit (modified from Masini et al., 2010a, 2010b), b) the radiolarites and slates unit, and c) the grey limestones unit. The sub-surface portion of the geological profile displayed in a) was constructed using the ''projecting faults to depth'' technique (Roeder et al., 1978). An oblique to bedding fault in the north-northeast part of this profile was removed because it shown a certain amount of movement out of the section. The beds in the hangingwall of this fault were redrawn in order to display a geologically reasonable reconstruction of the structure. The profiles are displayed from bottom a) to top c). The profile in a) is derived from the geological section across the mechanical unit 1 in figure 3b, the profile in b) from the geological section across the mechanical unit 2 in figure 3b, and the profile in c) from the geological section across the mechanical unit 4 in figure 3b. Shaded area in b) illustrates the portion of the outcrop used to carry out the shortening and layer-parallel strain estimations.

Figure 7: Geometrical analysis of two ramp folds from the studied outcrop using the interlimb angle versus thrust ramp dip graphs designed by Jamison (1987). The black dots correspond to: a) the fault-propagation fold that involves the griotte limestones

unit, and b) a fault-bend fold that involves the grey limestones unit. Both graphs are displayed at the same scale. The data have been collected from the geological profiles depicted in figures 6a and 6c respectively. To measure the interlimb angle and the thrust dip both fold limbs, as well as the thrust, have been approximated by straight lines.

Figure 8: Fault displacement analysis of two ramp folds from the studied outcrop using the graph designed by Chapman and Williams (1984). The parameters plotted are the displacement on the fault for different horizons versus the distance from each cut-off point to an arbitrary reference point measured on the fault. a) Fault-propagation fold that involves the griotte limestones unit (data partially taken from Masini et al, 2010a, 2010b), and b) a fault-bend fold that involves the grey limestones unit. The data have been collected from the geological profiles depicted in figures 6a and 6c respectively.

Figure 9: Shortening and depth to detachment estimations using the lost area diagram (Epard and Groshong, 1993) for the: a) fault-propagation fold developed in the griotte limestones unit depicted in figure 6a, c) one of the detachment folds developed in the radiolarites and slates unit depicted in figure 6b, and e) one of the fault-bend folds developed in the grey limestones unit depicted in figure 6c. Plots of percentage of layer-parallel strain for different horizons for the: b) fault-propagation fold developed in the griotte limestones unit (Fig. 6a), d) one of the detachment folds developed in the radiolarites and slates unit (Fig. 6b), and f) one of the fault-bend folds developed in the grey limestones unit (Fig. 6c). The arbitrary reference level used to construct the lost area diagrams is the lower detachment in the case of the ramp folds and the upper detachment in the case of the detachment folds.

Figure 10: Strain values and distribution, using the Masini et al. (2010a) methodology, for the profiles displayed in figure 6 of the: a) fault-propagation fold developed in the griotte limestones unit, b) detachment folds developed in the radiolarites and slates unit, and c) fault-bend folds developed in the grey limestones unit. The profiles are displayed from bottom a) to top c).

Figure 11: Graph of variation of anticline core area versus shortening for symmetrical (chevron) and asymmetrical (kink) detachment folds with different ratios of backlimb length/forelimb length formed solely by limb rotation. The greater this ratio the more asymmetrical the anticline. The functions illustrate the whole evolution of the anticlines, from their initiation (shortening and core area equal to zero) up to the point in which they become isoclinal (core area equal to zero) assuming that the backlimb versus forelimb length ratio remains constant. The forward models of detachment anticlines have been constructed according to Hardy and Poblet (1994) theory using the software Detach (Wilkerson et al., 2004). The fold core area versus shortening graphs for detachment folds are inspired in those presented by Poblet and McClay (1996) and Poblet et al. (2004).

Figure 12: Stratigraphic column of the studied outcrop showing the distribution of the different types of fault-related folds and detachments, and the main features of the structures developed within each mechanical unit. The forelimb dip, interlimb angle, percentage of forelimb thickening with respect to backlimb thickness, percentage of hinge thickening with respect to backlimb thickness and percentage of layer-parallel strain refer to the most representative fault-related folds analysed in figures 7, 8 and 9. In the case of the layer-parallel strain, absolute values have been used.

Figure 13: Graph relating the average percentage of layer-parallel strain, the forelimb average dip, the inverse of the ellipticity coefficient multiplied by 10, the supplementary angle of the interlimb angle and the average percentage of forelimb thickening and hinge thickening with respect to the backlimb thickness for the fault-propagation fold involving the griotte limestones unit analysed in figures 7, 8 and 9, the detachment fold involving the radiolarites and slates unit analysed in figure 9, and the fault-bend fold affecting the grey limestones unit analysed in figures 7, 8 and 9. These fault-related folds are illustrated in figure 6 and the data have been taken from figure 12. In the case of the layer-parallel strain, absolute values have been used.

Figure 14: Triangular graph relating the structure dimensions, located in the vertices of the triangle (large-scale structures involving the whole mechanical unit, small-scale structures involving some beds and combination of both), and three parameters used to define the different mechanical units, displayed as different sectors within the triangle (presence or absence of a basal detachment, lithological monotony or alternation of lithologies of different competence, and smoothness or roughness of the bedding surfaces). The position of the boundaries between the different parameters is conceptual. The triangle has been constructed considering only the situations observed in the studied outcrop.

Figure 15: Triangular graph relating different stratigraphic and rheologic parameters (displayed as sectors within the triangle) versus different types of fault-related folds (located in the vertices of the triangle). The position of the boundaries between the different degrees or intensities of each stratigraphic and rheologic parameter is

conceptual. The triangle has been constructed considering only the situations observed in the studied outcrop.

ACCEPTED MANUSCRIPT

TABLE CAPTIONS

Table 1: Values of height above the detachment for the fault-propagation and fault-bend fold and below the detachment for the detachment fold (H), unfolded bed length (L1) and width of the structure (W) measured in the geological profiles illustrated in figure 6, shortening (S) estimated using the lost area diagram in figure 9, and bed length before deformation (Lo) and percentage of layer-parallel strain (% Lps) estimated using equations (1) and (2). These values have been estimated for different horizons within: a) the fault-propagation fold developed in the griotte limestones unit, b) a detachment fold developed in the radiolarites and slates unit, and c) a fault-bend fold developed in the grey limestones unit.

FAULT-PROPAGATION FOLD (GRIOTTE LIMESTONES)							DETACHMENT FOLD (RADIOLARITES AND SLATES)							FAULT-BEND FOLD (GREY LIMESTONES)						
Horizon	H	L1	W	S	Lo	% Lps	Horizon	H	L1	W	S	Lo	% Lps	Horizon	H	L1	W	S	Lo	% Lps
H	3.64	16.63	13.45	4.37	17.82	-6.69														
G	3.42	16.86	13.45	4.37	17.82	-5.40														
F	3.29	17.03	13.45	4.37	17.82	-4.45	F	0,16	2.28	2.06	1.00	3.07	-25.64							
E	2.85	17.62	13.45	4.37	17.82	-1.14	E	0.25	2.27	2.09	1.00	3.08	-26.22	E	0.73	5.67	5.44	0.39	5.83	-2.71
D	2.33	17.84	13.45	4.37	17.82	0.10	D	0.44	2.48	2.11	1.00	3.11	-20.41	D	0.67	5.66	5.44	0.39	5.83	-2.92
C	1.60	17.98	13.45	4.37	17.82	0.88	C	0.58	2.67	2.10	1.00	3.10	-13.96	C	0.63	5.72	5.44	0.39	5.83	-1.87
B	0.67	17.92	13.45	4.37	17.82	0.54	B	0.72	2.97	2.11	1.00	3.11	-4.52	B	0.49	5.78	5.44	0.39	5.83	-0.83
A	0.01	17.70	13.45	4.37	17.82	-0.67	A	0.86	2.85	2.09	1.00	3.09	-7.88	A	0.25	5.75	5.44	0.39	5.83	-1.44

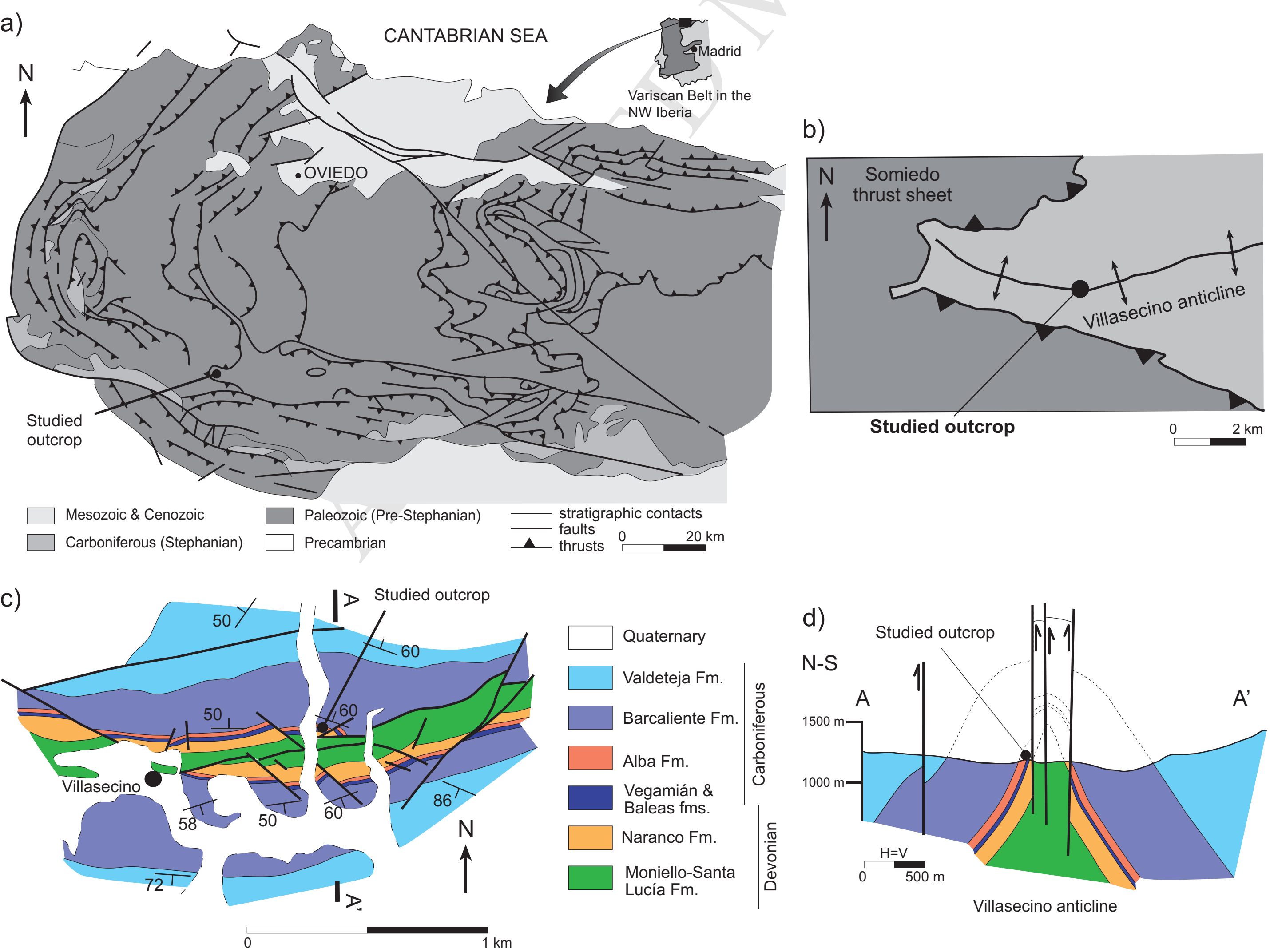
a)
CANTABRIAN SEA
N
Madrid
Variscan Belt in the NW Iberia
OVIEDO
Studied outcrop
Mesozoic & Cenozoic
Carboniferous (Stephanian)
Paleozoic (Pre-Stephanian)
Precambrian
stratigraphic contacts
faults
thrusts
0
20 km
b)
N
Somiedo thrust sheet
Villasecino anticline
Studied outcrop
0
2 km
c)
Studied outcrop
A
50
60
50
60
Villasecino
58
50
60
86
72
A'
N
0
1 km
Quaternary
Valdeteja Fm.
Barcaliente Fm.
Alba Fm.
Vegamián & Baleas fms.
Naranco Fm.
Moniello-Santa Lucía Fm.
Carboniferous
Devonian
d)
Studied outcrop
N-S
A
A'
1500 m
1000 m
H=V
0
500 m
Villasecino anticline

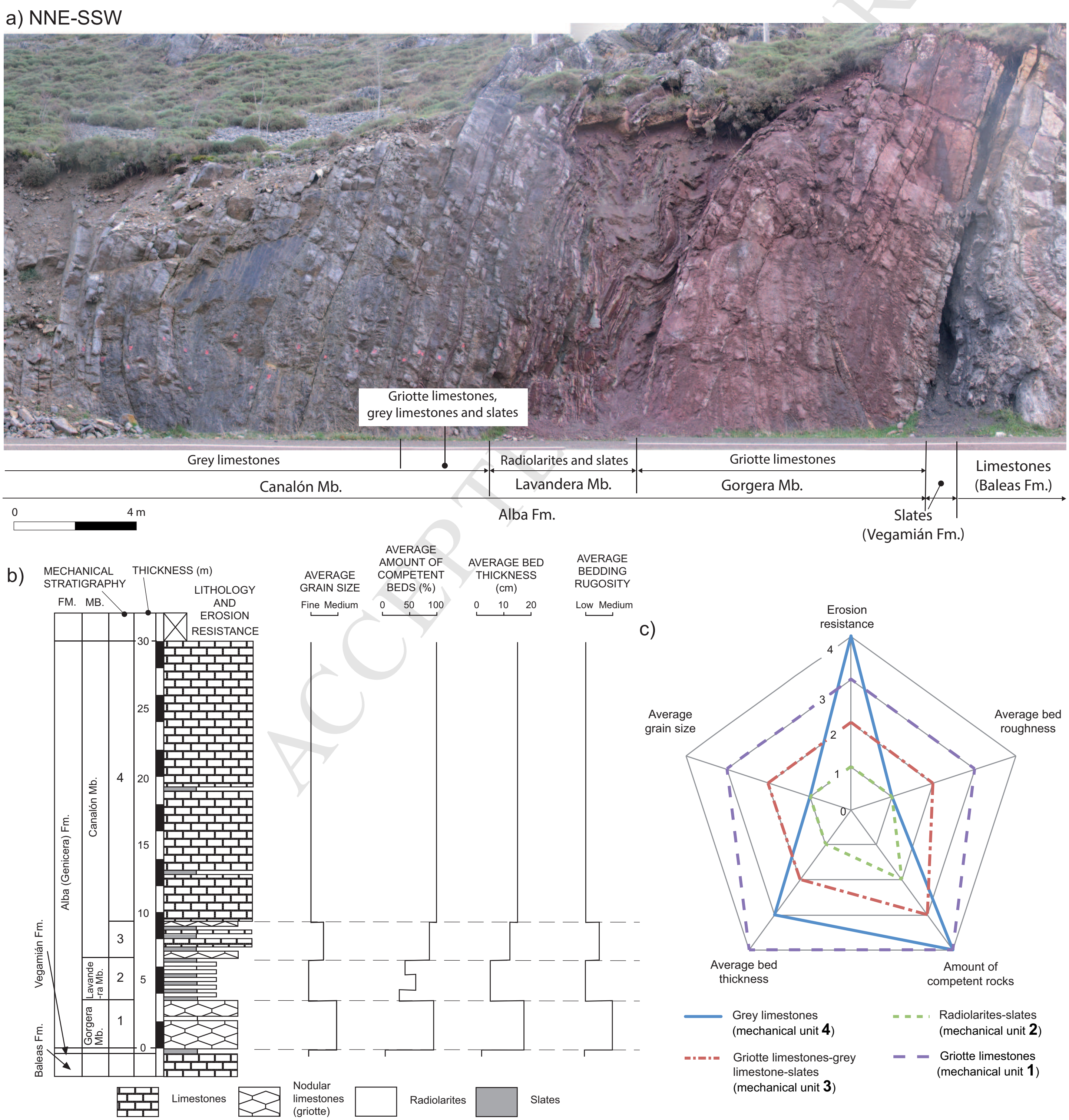

a) NNE-SSW
Griotte limestones, grey limestones and slates
Grey limestones
Radiolarites and slates
Griotte limestones
Canalón Mb.
Lavandera Mb.
Gorgera Mb.
Limestones (Baleas Fm.)
0
4 m
Alba Fm.
Slates (Vegamián Fm.)
b)
MECHANICAL STRATIGRAPHY
THICKNESS (m)
FM.
MB.
LITHOLOGY AND EROSION RESISTANCE
AVERAGE GRAIN SIZE
Fine Medium
AVERAGE AMOUNT OF COMPETENT BEDS (%)
0 50 100
AVERAGE BED THICKNESS (cm)
0 10 20
AVERAGE BEDDING RUGOSITY
Low Medium
Alba (Genicera) Fm.
Canalón Mb.
Lavande -ra Mb.
Gorgera Mb.
Vegamián Fm.
Baleas Fm.
4
3
2
1
30
25
20
15
10
5
0
Limestones
Nodular limestones (griotte)
Radiolarites
Slates
c)
Erosion resistance
Average bed roughness
Amount of competent rocks
Average bed thickness
Average grain size
0
1
2
3
4
Grey limestones (mechanical unit 4)
Griotte limestones-grey limestone-slates (mechanical unit 3)
Radiolarites-slates (mechanical unit 2)
Griotte limestones (mechanical unit 1)

a)


NNE
SSW
?
0
2 m

b)

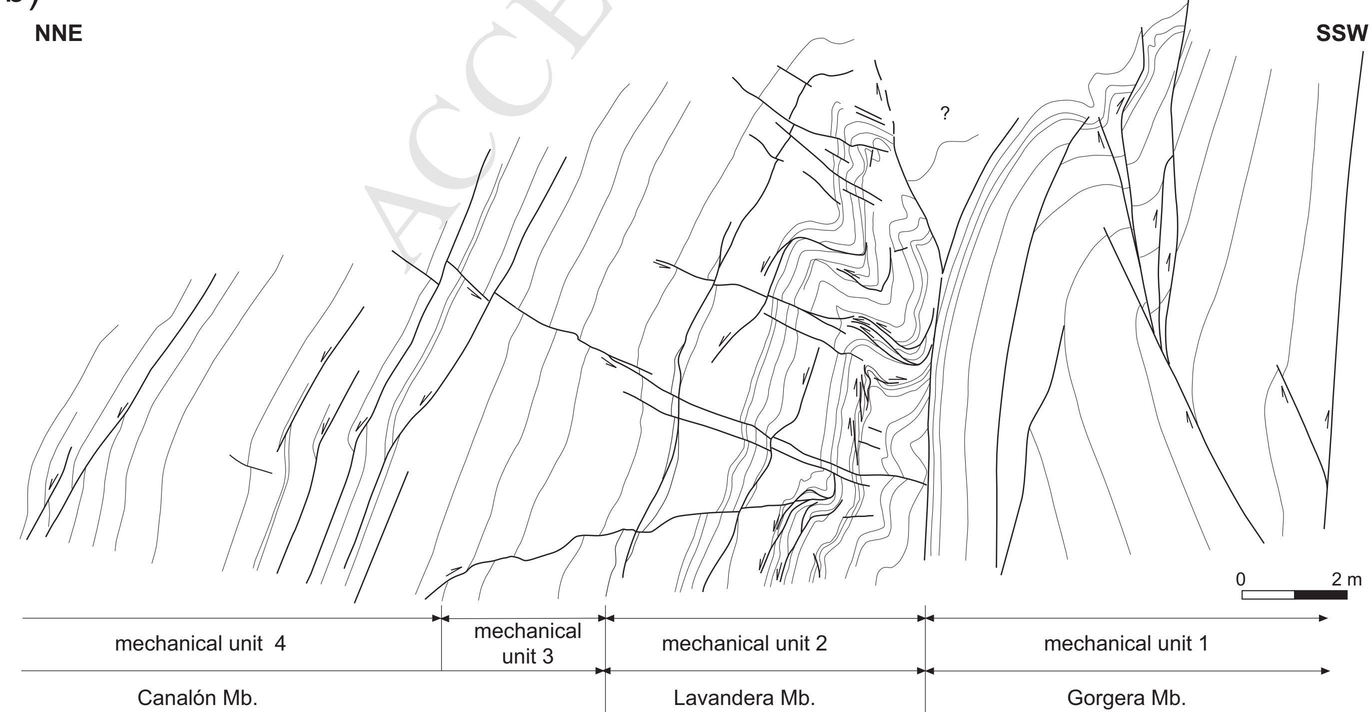
NNE
SSW
?
0
2 m
mechanical unit 4
mechanical unit 3
mechanical unit 2
mechanical unit 1
Canalón Mb.
Lavandera Mb.
Gorgera Mb.

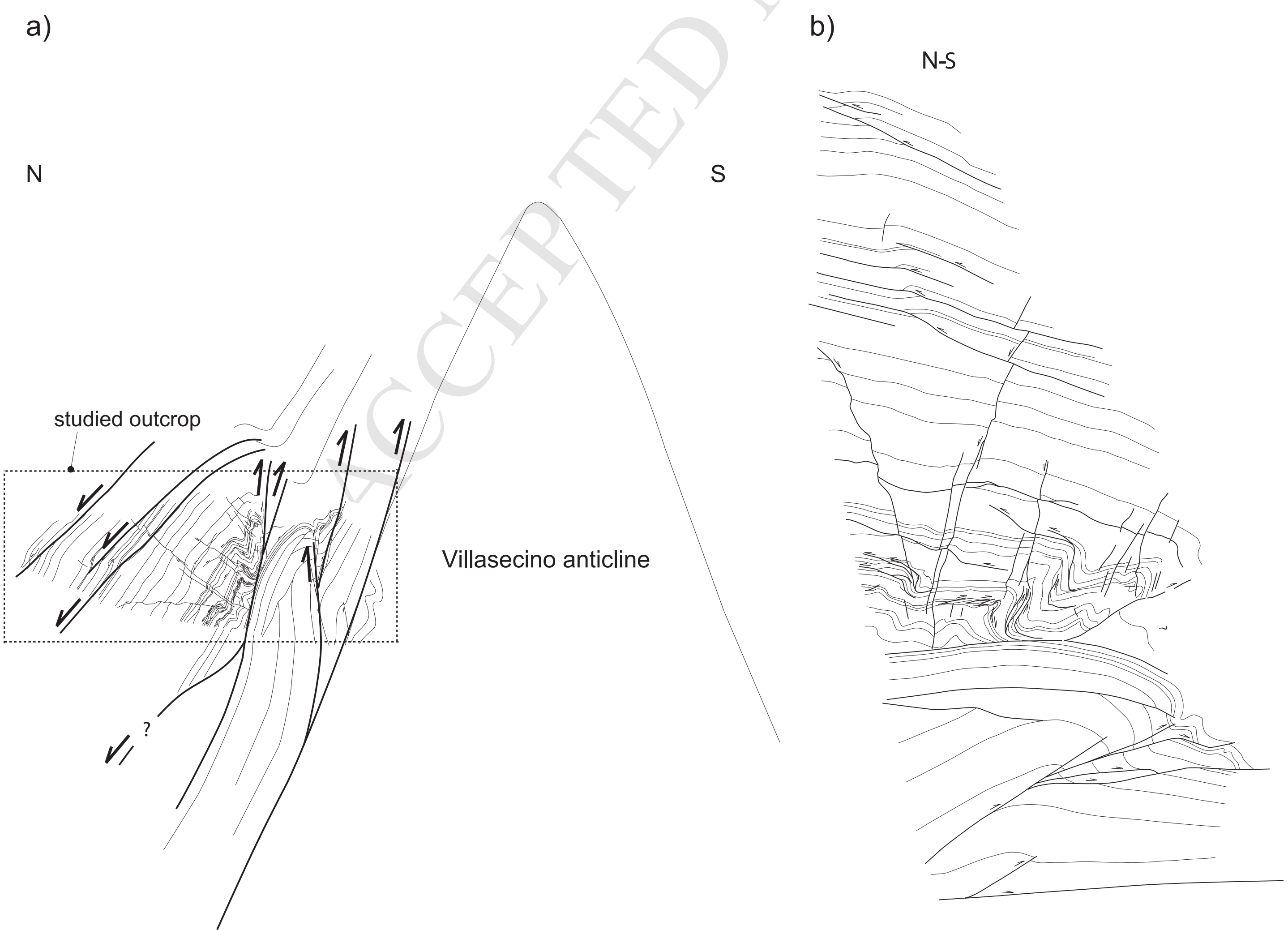
a)
N
S
studied outcrop
Villasecino anticline
?
b)
N-S

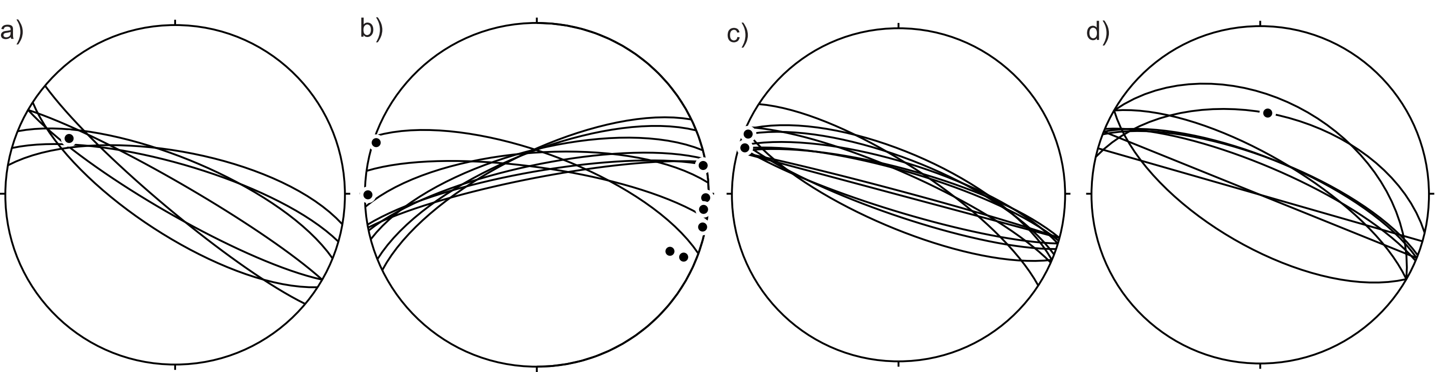
a)
b)
c)
d)

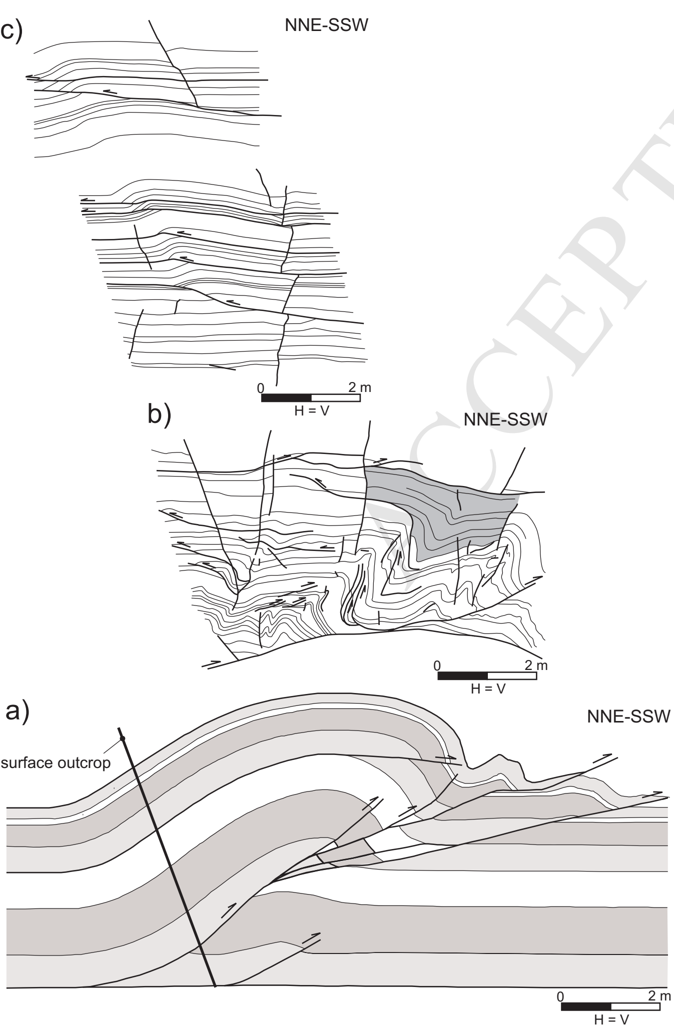

c)
NNE-SSW
0
2 m
H = V
b)
NNE-SSW
0
2 m
H = V
a)
NNE-SSW
surface outcrop
0
2 m
H = V

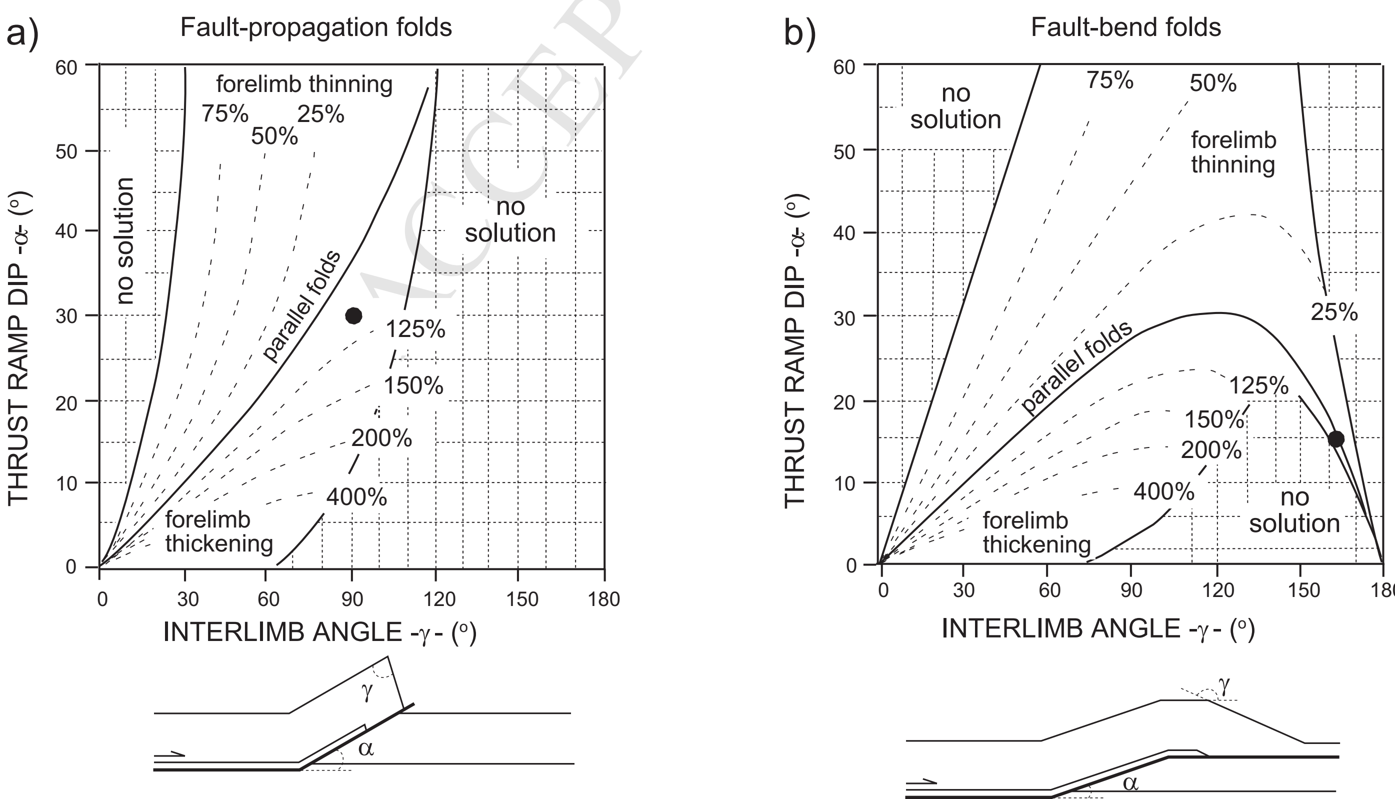

a)
Fault-propagation folds
THRUST RAMP DIP -α- (°)
INTERLIMB ANGLE -γ- (°)
no solution
forelimb thinning
75%
50%
25%
parallel folds
no solution
125%
150%
200%
400%
forelimb thickening
γ
α
b)
Fault-bend folds
THRUST RAMP DIP -α- (°)
INTERLIMB ANGLE -γ- (°)
no solution
75%
50%
forelimb thinning
25%
parallel folds
125%
150%
200%
400%
forelimb thickening
no solution
γ
α

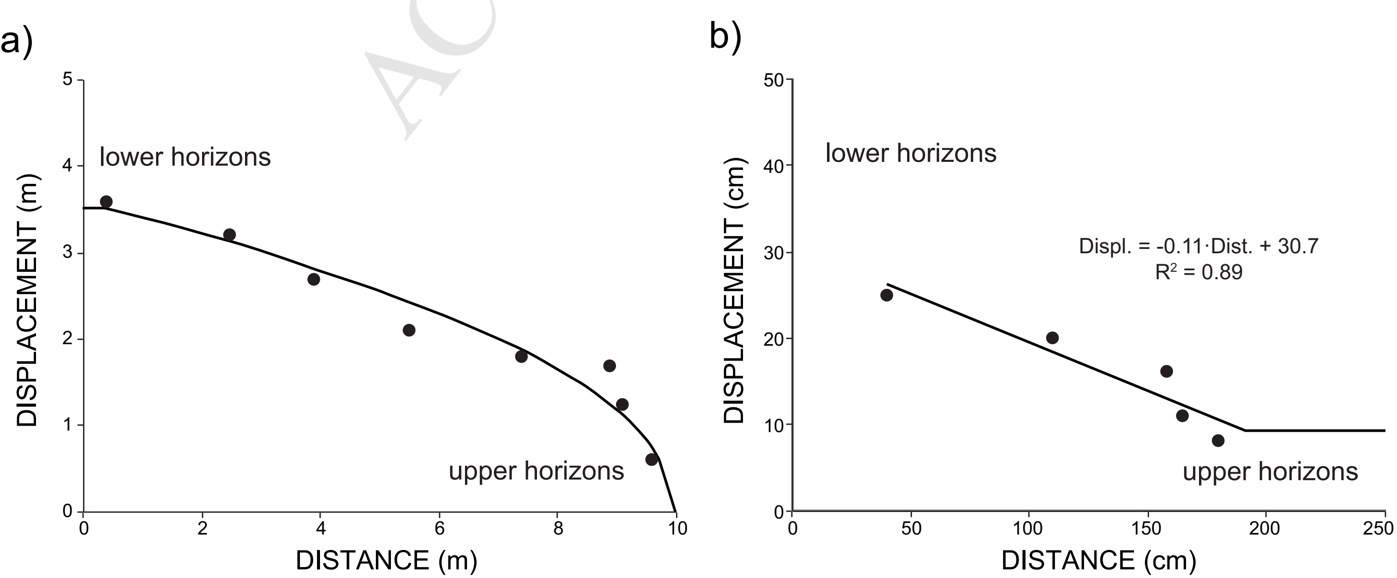
a)
lower horizons
upper horizons
DISPLACEMENT (m)
DISTANCE (m)
0
1
2
3
4
5
0
2
4
6
8
10
b)
lower horizons
Displ. = -0.11·Dist. + 30.7
R² = 0.89
upper horizons
DISPLACEMENT (cm)
DISTANCE (cm)
0
10
20
30
40
50
0
50
100
150
200
250

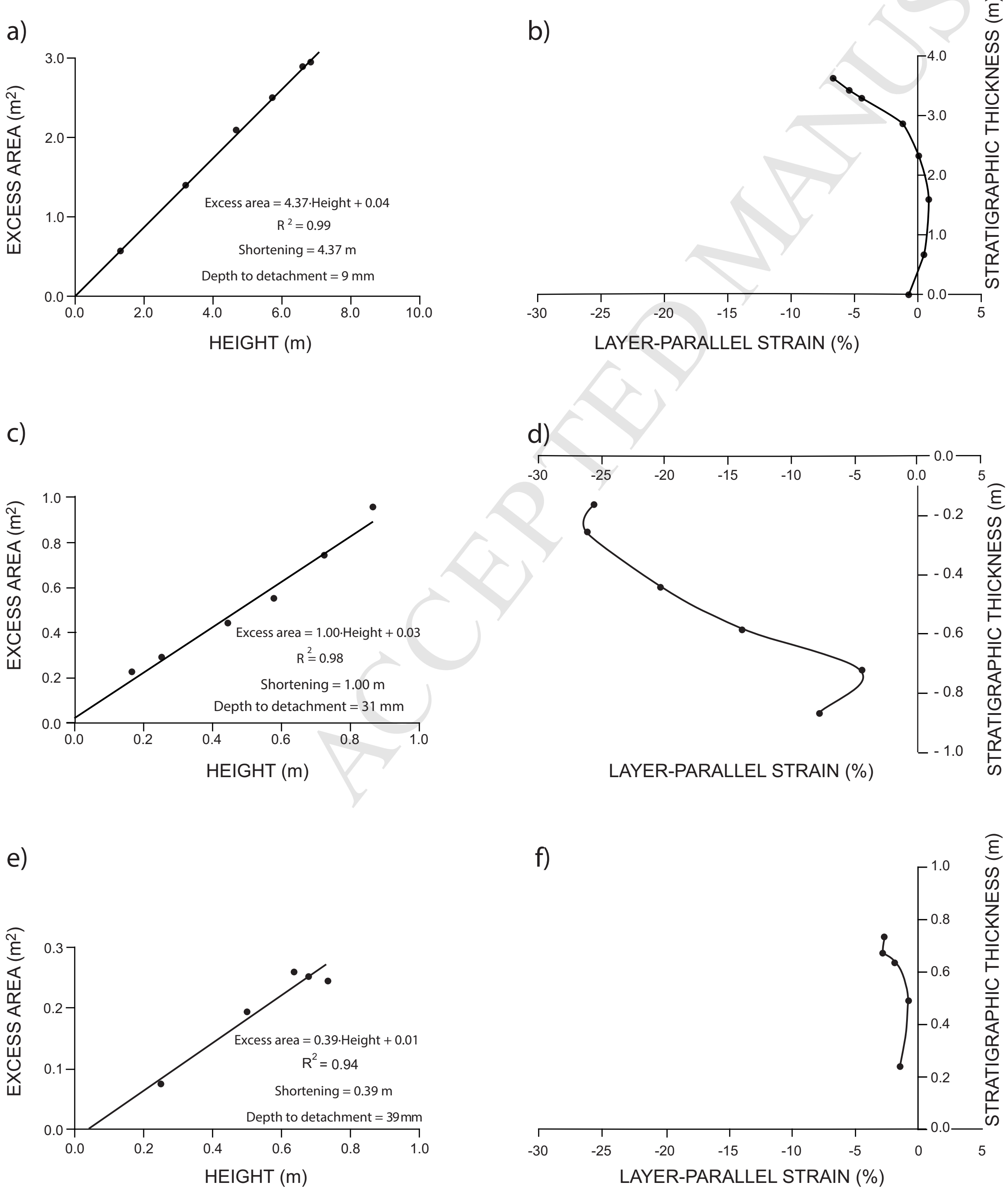
a)
EXCESS AREA (m2)
HEIGHT (m)
Excess area = 4.37·Height + 0.04
R 2 = 0.99
Shortening = 4.37 m
Depth to detachment = 9 mm
b)
STRATIGRAPHIC THICKNESS (m)
LAYER-PARALLEL STRAIN (%)
c)
Excess area = 1.00·Height + 0.03
R2 = 0.98
Shortening = 1.00 m
Depth to detachment = 31 mm
d)
e)
Excess area = 0.39·Height + 0.01
R2 = 0.94
Shortening = 0.39 m
Depth to detachment = 39mm
f)

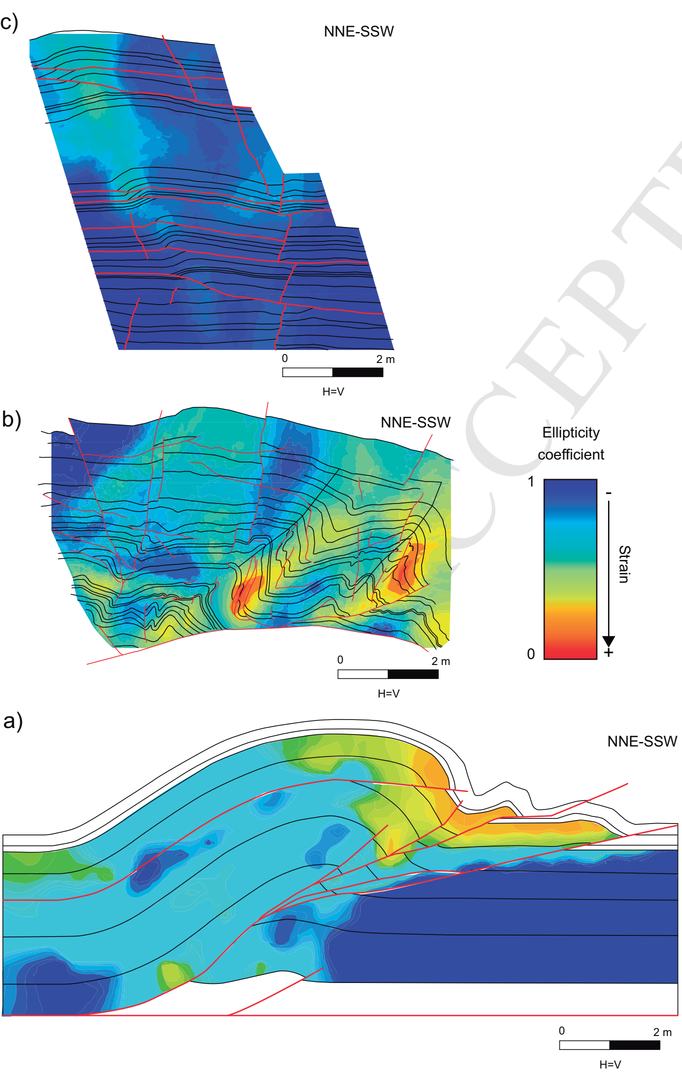
c)
NNE-SSW
0
2 m
H=V
b)
NNE-SSW
0
2 m
H=V
Ellipticity
coefficient
1
0
-
+
Strain
a)
NNE-SSW
0
2 m
H=V

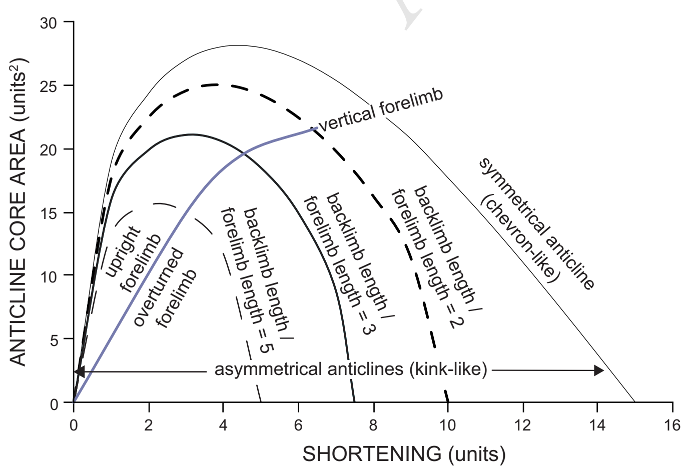

30
25
20
15
10
5
0
0
2
4
6
8
10
12
14
16
ANTICLINE CORE AREA (units²)
SHORTENING (units)
vertical forelimb
symmetrical anticline (chevron-like)
backlimb length / forelimb length = 2
backlimb length / forelimb length = 3
backlimb length / forelimb length = 5
upright forelimb
overturned forelimb
asymmetrical anticlines (kink-like)

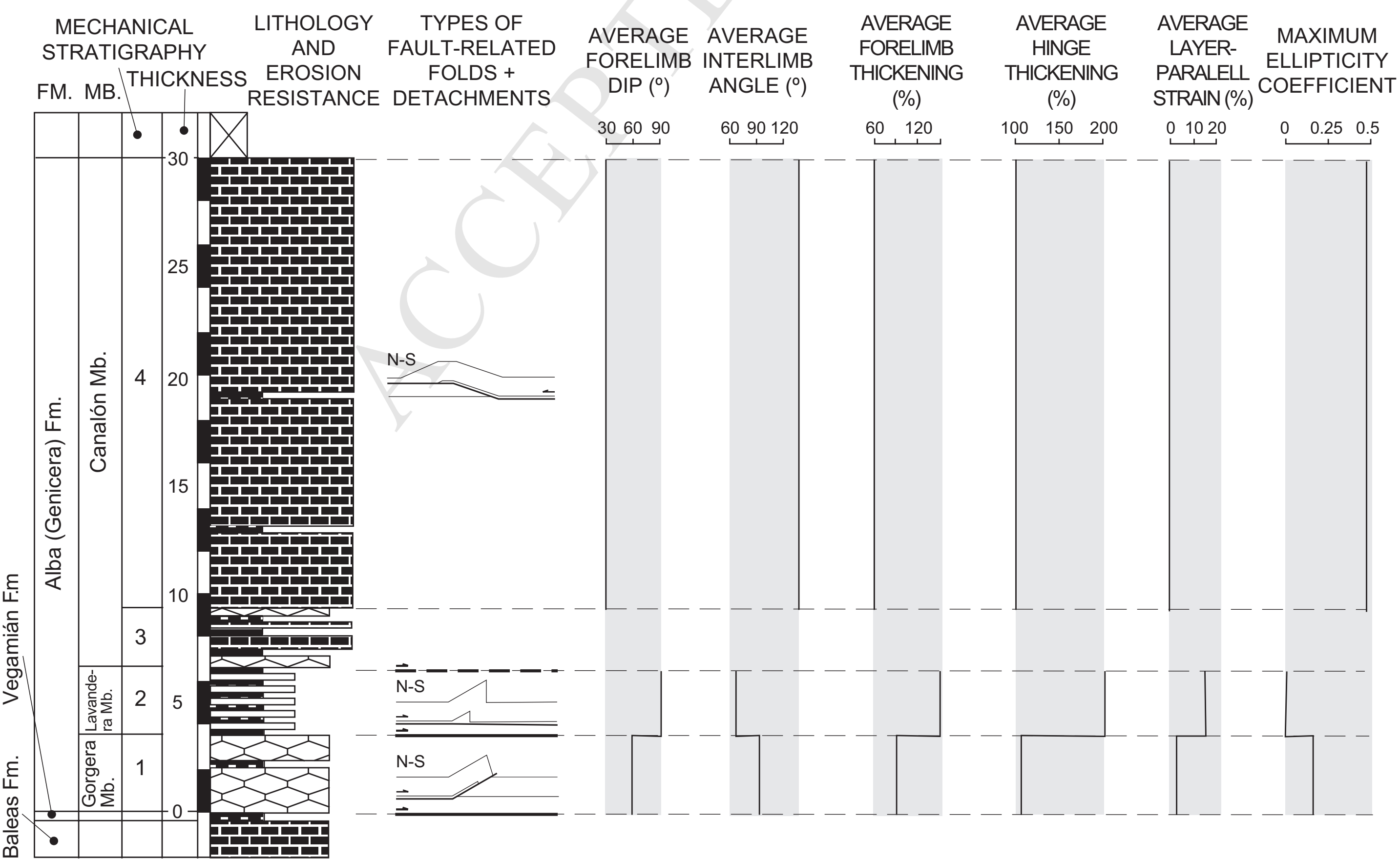
MECHANICAL STRATIGRAPHY
FM.
MB.
THICKNESS
LITHOLOGY AND EROSION RESISTANCE
TYPES OF FAULT-RELATED FOLDS + DETACHMENTS
AVERAGE FORELIMB DIP (º)
AVERAGE INTERLIMB ANGLE (º)
AVERAGE FORELIMB THICKENING (%)
AVERAGE HINGE THICKENING (%)
AVERAGE LAYER-PARALELL STRAIN (%)
MAXIMUM ELLIPTICITY COEFFICIENT
30 60 90
60 90 120
60 120
100 150 200
0 10 20
0 0.25 0.5
Alba (Genicera) Fm.
Canalón Mb.
Lavande-ra Mb.
Gorgera Mb.
Vegamián Fm
Baleas Fm.
1
2
3
4
0
5
10
15
20
25
30
N-S

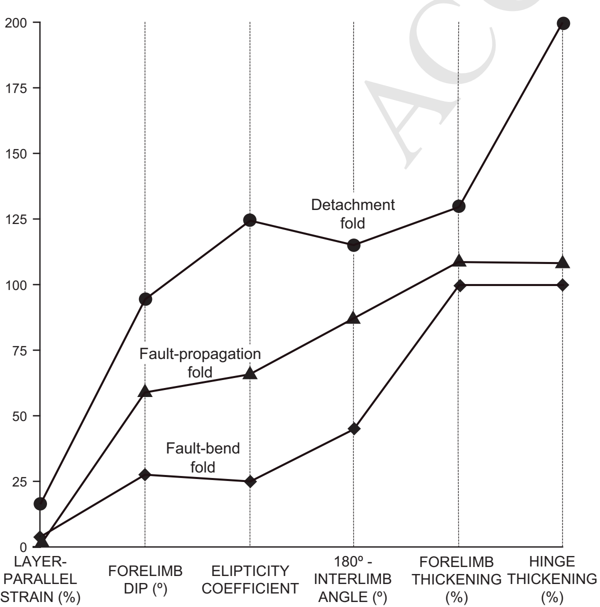
200
175
150
125
100
75
50
25
0
Detachment
fold
Fault-propagation
fold
Fault-bend
fold
LAYER-
PARALLEL
STRAIN (%)
FORELIMB
DIP (º)
ELIPTICITY
COEFFICIENT
180º -
INTERLIMB
ANGLE (º)
FORELIMB
THICKENING
(%)
HINGE
THICKENING
(%)

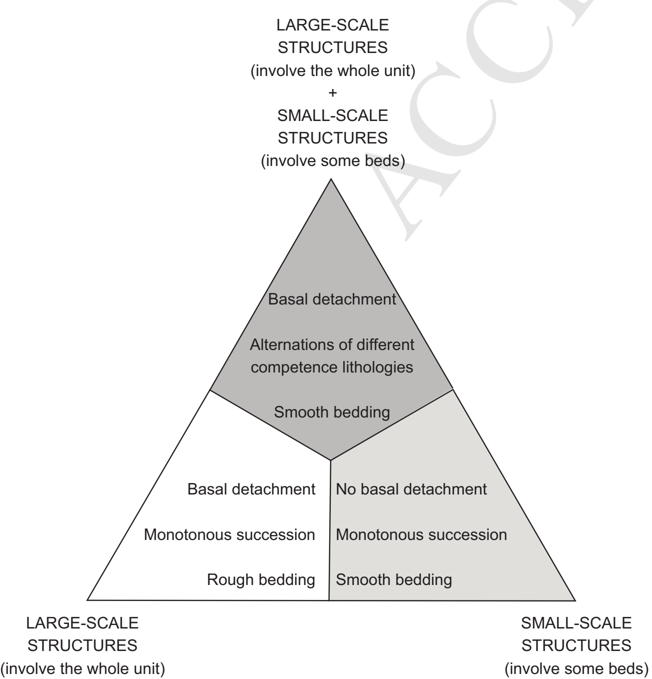
LARGE-SCALE
STRUCTURES
(involve the whole unit)
+
SMALL-SCALE
STRUCTURES
(involve some beds)
Basal detachment
Alternations of different
competence lithologies
Smooth bedding
Basal detachment
Monotonous succession
Rough bedding
No basal detachment
Monotonous succession
Smooth bedding
LARGE-SCALE
STRUCTURES
(involve the whole unit)
SMALL-SCALE
STRUCTURES
(involve some beds)

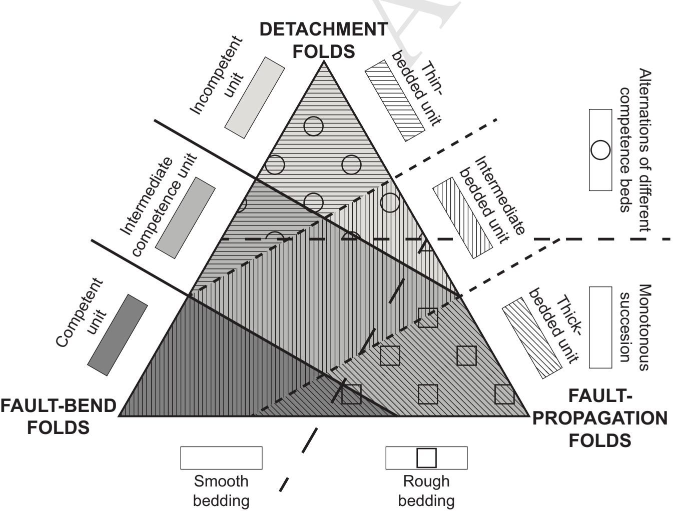
DETACHMENT
FOLDS
Incompetent
unit
Thin-
bedded unit
Intermediate
competence unit
Intermediate
bedded unit
Alternations of different
competence beds
Competent
unit
Thick-
bedded unit
Monotonous
succesion
FAULT-BEND
FOLDS
FAULT-
PROPAGATION
FOLDS
Smooth
bedding
Rough
bedding

- An outcrop, where different types of fault-related folds appear, is analysed
- The outcrop is located in the Cantabrian Zone (NW Iberian Peninsula)
- Three mechanical units can be differentiated
- The influence of several factors on the different structural styles is assessed
- Alike deformation conditions led to diverse structures depending on the rheology